p.52

PHOTOELECTROCHEMICAL FABRICATION OF SPECTROSCOPIC DIFFRACTION GRATINGS - PHASE II

FINAL REPORT
SBIR Phase II Research
For Period April 17, 1987 to August 17, 1989

CONTRACT NO. NAS5-30086

R. David Rauh, Principal Investigator
Michael M. Carrabba
Jianguo Li
Robert F. Cartland
John P. Hachey
Sam Mathew

EIC Laboratories, Inc.
111 Downey Street
Norwood, Massachusetts 02062
Telephone: (617) 769-9450

Prepared for

NASA/Goddard Space Flight Center
Greenbelt, Maryland 20771

February, 1990

TABLE OF CONTENTS

LIST OF FIGURES

LIST OF FIGURES
(Continued)

LIST OF TABLES

1.0 INTRODUCTION

Diffraction gratings are critical components in many of NASA's space missions for the purpose of spectral analysis of light from steller and albeido sources and as optical reflectors, beam splitters and filters. For example, the space telescope imaging spectrograph contains a faint object spectrograph and camera and a high resolution spectrograph, each utilizing spectroscopic gratings. Missions such as Spacelab, infrared and x-ray astronomical observatories and the Extreme Ultraviolet Explorer all rely on spectrographic dispersive components to gain information about the composition of the universe.

Diffraction gratings are extremely sensitive optical components which require much care and precision in manufacture. Optical components in the space environment may undergo thermal stresses and be subjected to radiational and particulate fluxes not found on earth. Most gratings manufactured for terrestrial spectroscopy are fabricated from organic polymer, either as holographically exposed photoresist or as epoxy-based replicas. In general, polymers leave much to be desired with respect to mechanical hardness and thermally induced volume changes, which are factors even when a reflecting metallic thin film is applied.

Metal master gratings are frequently used to stamp replicas into polymers. Masters are generally ruled using a diamond tool in soft metal films (e.g. Al, Au) vapor deposited on optically flat glass substrates. The ruling process is very slow because of the number of grooves required for a grating of practical size and mechanical/vibrational limitations to the rate of scribing each groove with a ruling engine.

Deep, low pitch Echelle gratings are of particular interest to NASA to provide both wide spectral coverage and high resolving power. These gratings have triangular grooves, typically with depths and separations on the order of 10-20 μm. Their fabrication by burnishing can leave inhomogeneities on the groove walls due to the large amount of material that must be removed. Similarly, ruling each new groove introduces stresses on neighboring grooves which may lead to deformations. A general problem with ruling engines is that all mechanical systems have some degree of linear inaccuracies. Such inaccuracies are less of a problem with holographic gratings, but the latter do not have the required V-groove profile.

This program has been directed toward the production of Echelle diffraction gratings by a light-driven, electrochemical etching technique (photoelectrochemical etching). Etching is carried out in single crystal materials, and the differential rate of etching of the different crystallographic planes used to define the groove profiles. Etching of V-groove profiles was first discovered by us during the first phase of this project, which was initially conceived as a general exploration of photoelectrochemical etching techniques for grating fabrication. This highly controllable V-groove etching process was considered to be of high significance for producing low pitch Echelles, and provided the basis for a more extensive Phase II investigation.

2.0 PHOTOELECTROCHEMICAL ETCHING OF ECHELLE STRUCTURES IN GaAs

2.1 General Background

Photoelectrochemistry is a general category encompassing light-induced electrochemical reactions of semiconductors in contact with liquid electrolytes arising from the primary generation of minority carriers. In the field of electronics and electro-optics, photoelectrochemical processing has been a subject of considerable recent interest. Photoelectrochemical etching has been used in the fabrication of diffraction gratings, integral lenses for light emitting diodes, fiber optic couplers, and via holes in a variety of semiconductor materials. Photoelectrochemically induced electroplating has been employed for both ohmic and non-ohmic contacts. Photoelectochemistry has also been used in the modification of semiconductor surfaces to reduce surface state densities prior to device fabrication.

When immersed in an electrolyte, a semiconductor undergoes an exchange of electrons with the liquid at the interface to equalize the work functions of the two phases. The result is often a rectifying barrier between the semiconductor and liquid that has properties similar to a metal-semiconductor "Schottky barrier", familiar in solid state electronics. The contact barrier that is produced is characterized by a bending of the semiconductor's conduction and valence bands. Such barriers are well known to be photoactive. Thus, when light of energy greater than the bandgap strikes the interface and is absorbed by the semiconductor, electrons and holes are produced, with minority carriers being swept to the semiconductor surface. In the case of n-type semiconductors, these minority carriers are valence band holes which, upon arrival at the interface, can be consumed by a chemical reaction with the electrolyte or by (non-productive) surface recombination with majority carriers. For most technologically significant semiconductors (Si, Ge, III-V and II-VI compounds), valence band holes are sufficiently energetic to decompose the semiconductor in aqueous media. This phenomenon forms the basis for the photoelectrochemical etching/micromachining process employed in grating fabrication.

Photoelectrochemical etching occurs only when an optically produced minority carrier at the semiconductor-electrolyte interface is sufficiently energetic to induce a corrosion reaction. This condition is met for valence band holes for virtually all semiconductors used in electronics in contact with aqueous electrolytes. In order for etching to occur at a sufficiently practical rate, kinetics must also be favorable. Processes which consume minority carriers without corrosion, such as surface recombination and reaction with dissolved electrolyte species, will detract from the overall quantum efficiency of etching by kinetic competition. Mass transfer can also kinetically inhibit the etching reaction. It is particularly important in this regard to employ an electrolyte in which the corrosion products are highly soluble.

Photoelectrochemical reactions are typically carried out in a photoelectrochemical cell in which the electrochemical potential of the semiconductor may be controlled and the current monitored and integrated. An ohmic contact is provided onto the semiconductor's backside, not exposed to the electrolyte, through which connection to the external circuit is made. The potential of the semiconductor is varied versus a standard reference electrode potential using a potentiostat. The current flowing between the semiconductor "working" electrode and an auxiliary "counter" electrode is recorded as a function of potential and/or time, and integrated using a coulometer.

In a photoelectrochemical reaction with unit quantum yield, each photon absorbed by the semiconductor will give rise to one electron in the dissolution process. In a well-behaved photoelectrochemical cell, the curve of photocurrent (or quantum yield) vs. applied potential is S-shaped, as shown schematically in Figure 1. As indicated by the band bending diagrams also shown in Figure 1, when the applied potential is negative of the flat band value (V_{fb}) for an n-type semiconductor, the bands are flat and there is little electron-hole separation, and hence negligible photocurrent. As a positive potential is applied, the bands become bent due to a surface depletion of electrons. A space charge layer is thus formed, the width and magnitude of which grows as the potential becomes more positive. Above a certain potential, the space charge region reaches a limiting width. The efficiency of separation of electron-hole pairs, and thus photocurrent production, also increases with voltage due to the fact that more pairs are created within the space charge region and the driving force for their separation increases. The plateau region of highest photocurrent quantum yield is often referred to as the photon limited region.

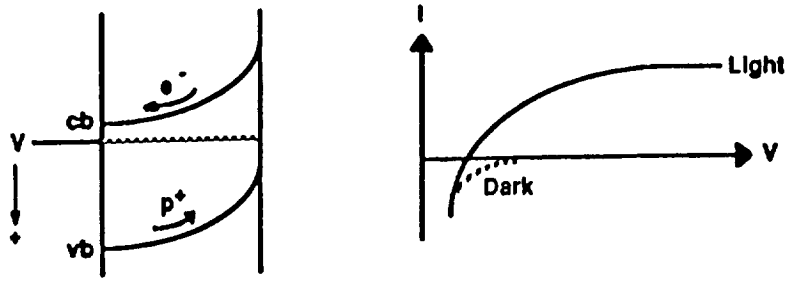

Figure 1. Idealized current-potential curve and band bending diagram for a n-type semiconductor in the dark and under illumination. Conduction and valence band are indicated (cb,vb).

The beauty of photoelectrochemical etching is that the rate of etching can be controlled by the photon flux and by the potential, due to the linear relationship between light intensity and photocurrent. Since an ampere is equal to a current of 6.24×10^{18} electrons/s, it can be shown that the current equivalent of photons is equal to $8.065 \times 10^{-5}\lambda I$ "photon amperes". The quantities λ and I are the wavelength (Angstroms) and intensity (watts/cm^2) of the light source. The rate of etching may be expressed quantitatively as

$$r(\mu/s) = 8.36x10^{-6}(1-R)\phi\lambda AI(m/n\rho) \qquad (1)$$

where R is the normal incidence reflectance of the crystal, and φ is the quantum yield of conversion of photons to current in the dissolution reaction. The quantity (m/nρ) describes the etching reaction, where m is the molecular weight of the dissolving layer, ρ is its density in g/cm^3, and n is the number of equivalents/mole in the dissolution process.

2.2 Gallium Arsenide Photoelectrochemical Etching

The material of choice for photoelectrochemical fabrication of diffraction gratings in this program was gallium arsenide (GaAs). The major reason for this choice was the ease of conducting photoelectrochemical dissolution in a variety of relatively mild electrolytic media, and its zinc-blend

crystal structure (see below). GaAs with n-type doping corrodes oxidatively when held at positive potentials and illuminated with light of energy greater than its optical bandgap ($\lambda < 873$ nm). Schematically, the reaction may be represented as a six electron oxidation, viz.

$$GaAs \Rightarrow Ga^{+3} + As^{+3} + 6e^{-}$$

The trivalent oxidation products hydrolyze in aqueous media to give oxyanions which are more or less soluble over a wide pH range. Thus, in many electrolytes, passivation products do not build up at the interface and suppress the progress dissolution.

2.3 Experimental Procedures

There are three major components in an apparatus for photoelectrochemical processing. First is the cell for exposing the semiconductor working surface to the electrolyte while also accommodating auxiliary electrodes for controlling the semiconductor potential. Second is the control apparatus, typically a potentiostat and a means for monitoring current and charge. Finally is a light source, which can be broad band or monochromatic laser radiation.

The choice of a cell will be largely dependent on the type of processing to be accomplished. We employed the cell shown in Figure 2 for etching diffraction gratings. The cell body should be machined from a polymer stable to the electrolyte of choice. The cell body was machined from nylon stock, which is adequate for many aqueous electrolytes. The semiconductor electrodes must be mounted in such a way to prevent contamination of the ohmic contact (or other corrosive elements) by the electrolyte. In the approach illustrated in Figure 2, the semiconductor "working" electrode incorporates an ohmic contact on the back side. The n-GaAs electrode was mounted onto a brass disk using conductive silver filled epoxy. The assembly was potted into a Kel-F holder with epoxy cement, save for a threaded hole in the rear of the brass disk. A screw assembly is used both as a contact and to tighten the electrode onto the cell via a liquid-tight O-ring seal. A cylindrical platinum gauze counter electrode surrounded the working electrode, giving rise to a uniform current distribution. A standard calomel (SCE) reference electrode is placed as close as possible to the electrode surface without occluding the light path.

The photoelectrochemical etching experiments were carried out on single crystal (100) GaAs substrates obtained from MA/COM Laser Diode Inc. and Bertram Laboratories. The crystals were Si-doped, n-type with carrier densities of 5×10^{17} and $6 \times 10^{18}/cm^3$. Ohmic contacts were made by rubbing Ga-In eutectic on the back side of the substrate before attaching it to a brass disk with silver-filled conducting epoxy. In these experiments, the electrode surface was lapped and polished successively with alumina polishing powders with particle size 20, 5, 1, 0.3 and 0.05 μm to obtain a mirror finish. The last step was a chemomechanical polishing with a Rodel 2360 silica slurry/bleach/water (1:1:10) mixture.

After polishing, the electrode was dried in an oven at 110°C. A positive photoresist (Shipley microposit S1400-31) was then spun onto the electrode surface at 7000 rpm and soft-baked at 95°C for 30 minutes. The photoresist etch mask was patterned by illumination with UV light through a periodic Cr/Au mask in contact with the electrode surface and aligned along the [01$\bar{1}$] direction. For most experiments, the mask had a periodicity of 50 lines/mm with a line/space ratio of 2. After the exposed photoresist was developed, the entire electrode surface was exposed again with UV

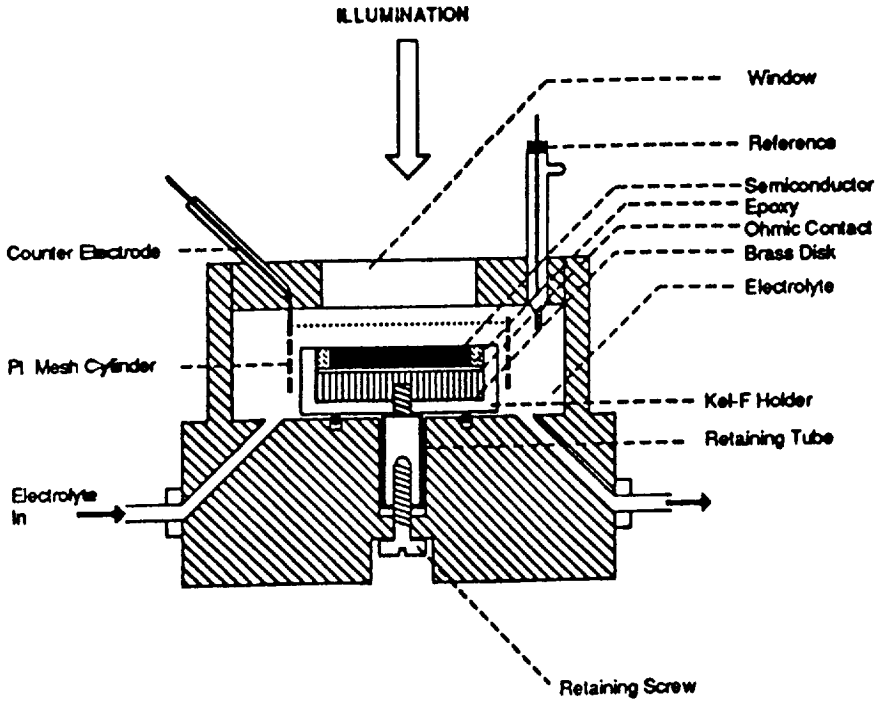

Figure 2. Cell design and GaAs mount for the fabrication of photoelectrochemically etched gratings.

light. The final step in the masking process was hard baking in air at 125°C for 45 minutes. The thickness of the mask determined with a Sloan Dektak profilometer was 1.5 ± 0.2 μm.

Photoelectrochemical etching was carried out in a 3-electrode configuration using an SCE reference electrode as described above. Unless otherwise noted, irradiation was provided using an Oriel 500W Hg(Xe) photoresist exposure illuminator with a ± 5% beam uniformity over a 20 cm^2 area. The filtering was such that the irradiation wavelength was distributed between 350-450 nm. Most experiments were conducted at an intensity of 30 mW/cm^2. In some experiments, the light was focused onto the electrode surface using a convex lens and adjusted to an intensity of 300 mW/cm^2.

2.4 Photoelectrochemically Etched Sawtooth Echelle Structures

The results of the first phase of this program and part of the second phase have been published in two papers, included as Appendices A and B. These results are summarized below.

The general approach for making periodic structures has been to employ a photoresist mask to define the photoetched pattern. The semiconductor is then photoelectrochemically etched in the exposed regions, after which the pattern mask is removed with a suitable solvent. In principle, the etching will occur vertically with the edges sharply defined by the edges of the mask. However, we demonstrated that crystallographic orientation, the masking material, the electrolyte, and the bulk semiconductor properties can have profound effects on the result.

The key observation was that n-GaAs exhibits a strong orientational effect on the photoanodic etching process. Orientational effects of photoanodic etching of n-GaAs were first examined in this laboratory using (100) crystals with a mask defining slots oriented along three primary directions, as shown in Figure 3. These structures were etched at a bias of 0.5V vs. SCE, and a broad band light intensity sufficient to yield a dissolution current of 10 mA/cm^2 in the electrolyte containing either 1M KCl or 0.3M Tiron (4,5-dihydroxy-1,3-benzene disulfonic acid) a Ga^{+3} complexant. The shape of the resulting photoetched trenches are shown in Figure 4. In both electrolytes, the Ga-rich crystallographic surfaces are preferentially exposed in grooves defined in the (100) surface along the [01$\bar{1}$] direction. The other directions exhibit more or less vertical etching.

While a similar effect can be produced with oxidizing chemical etchants, Br_2/methanol and H_2SO_4-H_2O_2-H_2O in GaAs, for example [1,2], or HF in silicon (which has a similar zinc-blend structure), photoelectrochemical etching has a major advantage. The rate and uniformity of etching can be controlled by both the light flux and the applied potential, and the development of microstructures can be monitored coulometrically.

In order to produce blazed Echelle gratings, it is necessary to cut the GaAs crystal at an angle off the (10$\bar{0}$) plane toward the (011) plane. As shown in Figure 5, orienting the photoresist lines in the [01$\bar{1}$]direction still gives rise to structures with the interior angles governed by the preferred Ga-rich surfaces. One advantage of photoelectrochemical etching for producing these structures is that the process can be followed coulometrically. The charge, Q, required to etch the V-groove sawtooth pattern is:

$$Q(C/cm^2) = 3.54x10^3 nN(0.5W^2/\cot(\alpha-\beta)+(\alpha+\beta)) \qquad (2)$$

Here, n is the electron stoichiometry (equivalents/mole) of the photoanodic dissolution reaction, W is the width (cm) of each groove, α is the angle of the groove face with respect to the (100) surface, β is the angle of the crystal slice with respect to the (100) surface, and N is the number of grooves/cm.

An example from this laboratory demonstrates the photoelectrochemical etching of blazed structures. Crystals of n-GaAs (N_D=5x10^{17}/cm^3) were cut and polished with (100), (100)-8° and (100)-18° orientations. The other parameters in equation (2) were: n=6, N=500 and W=2 x 10^{-3} cm. The electrolyte composition was 0.1M KCl, adjusted to pH 3, and the light intensity was 30 mW/cm^2. The potential was held at the onset of the photon limited region, 0.4V vs. SCE. Initial structures were etched under the assumption that the interior angles were 70.54°, as defined by the (111) Ga surfaces. However, we found under closer examination that this angle was dependent on the etching conditions and on the electrolyte, and was closer to 90° under the present conditions. This would correspond most closely to the (223)Ga-rich surface. With a 90° interior angle, equation (2) predicts a charge of 10.6 and 8.6 C/cm^2 required to etch the gratings in the (100) and (100)-18° surfaces, respectively. With coulometric monitoring, both unblazed and blazed gratings were produced with pointed tops and bottoms and extremely smooth walls. A scanning electron micrograph of the blazed structure from the (100)-18° surface is shown in Figure 6. The blaze angle of 60° is slightly less than the expected value of 63°, an error probably due to inaccuracies accumulated in the cutting and polishing procedures.

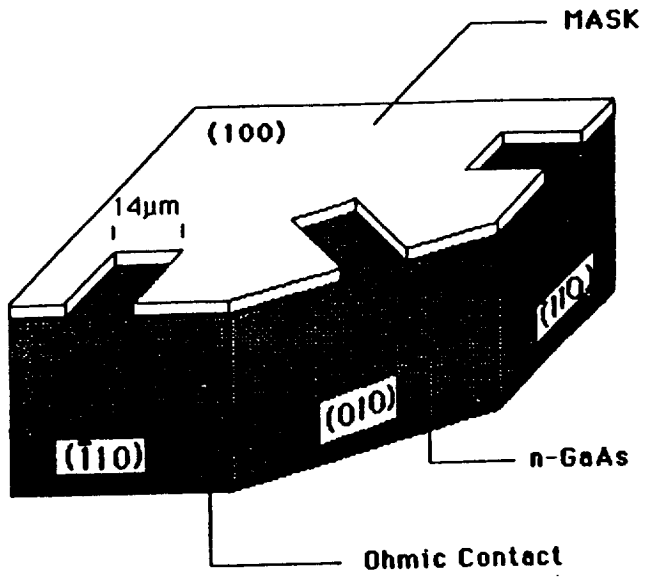

Figure 3. Patterning of (100) n-GaAs crystal surface for PEC etching of grooves.

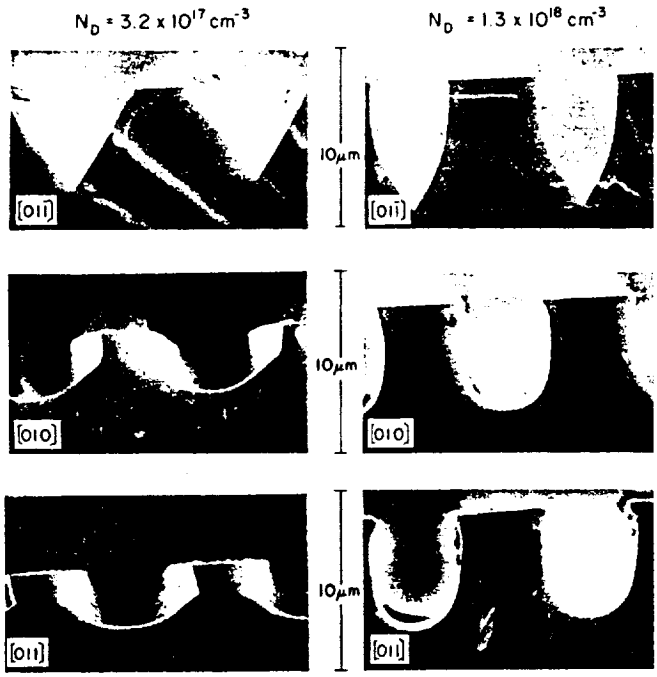

Figure 4. Scanning electron micrographs of cross sections of photoelectrochemically etched grooves in (100) n-GaAs, showing effects of groove orientation and doping level. Electrolyte is 0.5M Tiron; light source is 150W Xe, intensity adjusted to give photocurrent of ~20 mA/cm^2. Potential = -0.2V vs. SCE; charge = 11 C/cm^2.

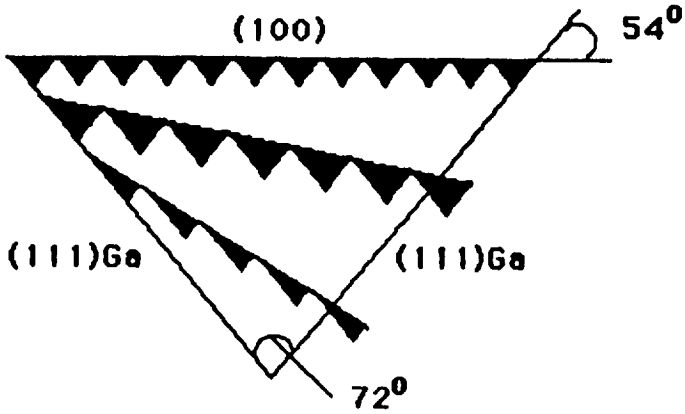

Figure 5. Schematic cross section of V-grooves arising from exposed [111]Ga planes for GaAs cut at various angles off (100) plane.

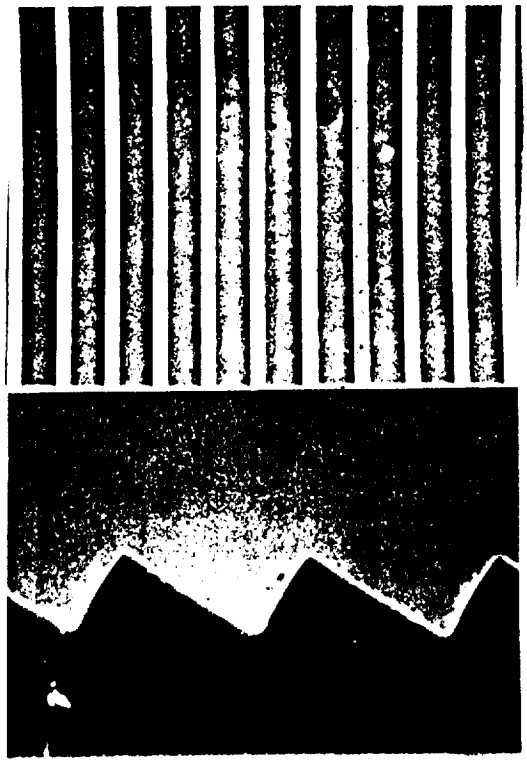

Figure 6. Scanning electron micrographs of blazed Echelle gratings etched photoelectrochemically in the (100)-18° surface of n-GaAs. Groove spacing is 20 μm.

3.0 PROCESS OPTIMIZATION

3.1 Effects of Electrolyte, Materials and Etching Parameters

The initial work on this program, described in the previous section, demonstrated that V-grooves could be produced by photoanodic etching in GaAs using a periodic mask to define the spacing [3,4,5]. Key to the process for etching symmetrical grooves is the alignment of the pattern on the (100) surface along the [01$\bar{1}$] direction. Furthermore, we have reported in other work the effect of doping and orientation on producing a wide variety of high aspect ratio groove profiles using opaque metal masks [6]. Such deep structures could not be readily achieved by wet chemical techniques, since light can be used to control the direction of etching. Matz has demonstrated similar orientational effects with maskless photoelectrochemical etching of gratings in GaAs and InP [7,8] by projecting interferograms onto the electrode surface.

The actual V-groove profiles have been assumed to arise from the exposure of (111)Ga planes. However, it became obvious during the course of our work that the groove angles and morphology had a dependence on electrolyte composition and other process parameters such as light intensity. Reported in this section are the results of investigations into the effects of supporting electrolyte, light intensity, doping density, applied potential and photoresist processing on the photoelectrochemically etched V-groove structures in n-GaAs.

Undercutting Beneath the Photoresist Mask. Figure 7 shows SEM micrographs of the V-grooves etched in 0.5M KCl using a light intensity of 30 mW/cm^2 after passage of 4 C/cm^2, about half the charge required to complete the etching of the grating. At this stage of the etching, no damage or liftoff of the photoresist mask was observed. There is clear evidence, however, that undercutting took place along the edges of the stripes of the photoresist mask with the assistance of light transmitted through the photoresist (Figure 7a). A 1.5μ thick photoresist film on a quartz substrate was determined by absorption spectroscopy to be >60% transmissive between 300 and 900 nm, where GaAs absorbs. During the photoetching, therefore, the GaAs covered with photoresist is illuminated as well as the exposed surface. The light penetrating the mask is responsible for undercutting the photoresist and eventual formation of the connected V-grooves.

Electrolyte Composition. Photoelectrochemical etching of V-grooves was done in neutral aqueous solutions with KCl, Na_2SO_4 and NaF as supporting electrolytes. Typical photocurrent vs. potential curves are shown in Figure 8. In 0.5M KCl or Na_2SO_4, the limiting photocurrent was proportional to the light intensity up to the highest intensity used (300 mW/cm^2) and remained steady with time. In 1M NaF at 30 mW/cm^2, however, the photocurrent decreased by nearly 80% over the same time period indicating passivation was taking place at the GaAs surface.

Figure 9 shows the SEMs of the V-grooves etched (100) GaAs (Nd = 5 x 10^{17}/cm^3) in 1M NaF, 0.5M Na_2SO_4 and 0.5M KCl, respectively. All three samples were produced under a light intensity of 30 mW/cm^2, at a bias of 0.4V vs. SCE. Both the shape and the surface texture of the V-grooves were affected by the composition of the electrolyte. A very shallow V-groove pattern with rough side walls was formed in the 1M NaF electrolyte. In addition, some precipitation of particles was observed at the bottom of the grooves in support of the surface passivation suggested

by the photocurrent decay. However, in 0.5M KCl electrolyte a well defined V-groove pattern with a relatively smooth interior wall was obtained. The V-groove etched in Na_2SO_4 had a rough interior wall, and the bottom of the groove did not reach a point.

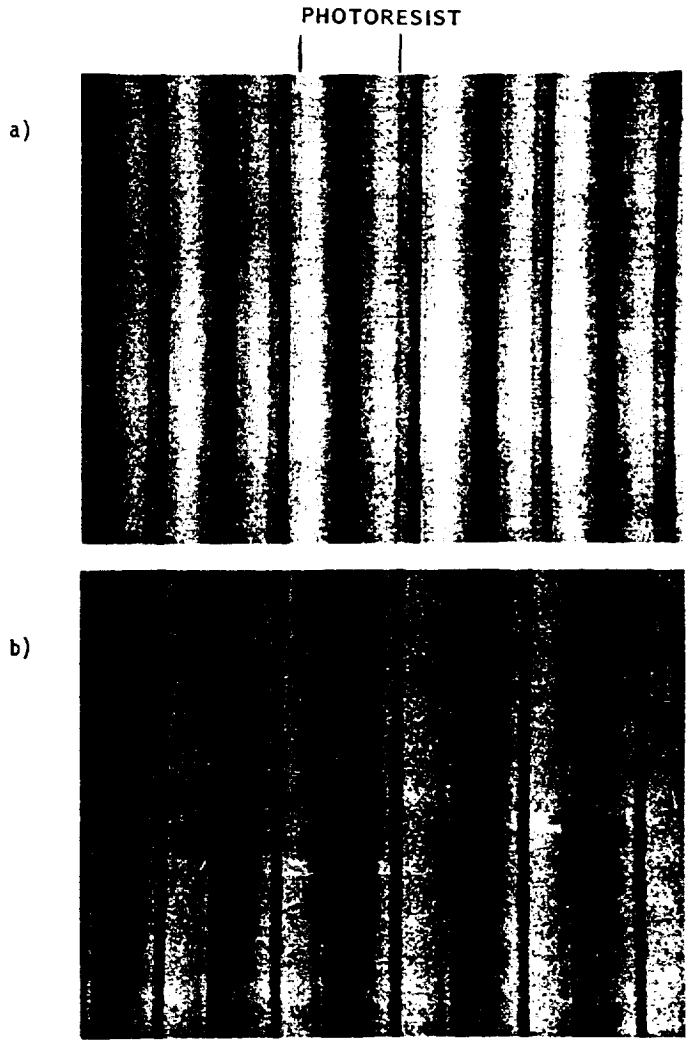

Figure 7. Undercutting of photoresist during photoelectrochemical etching of [01$\bar{1}$] oriented stripe pattern on (100) n-GaAs. Period = 20 μm.

Concentration of KCl. We observed a direct correspondence between the interior angle of the photoelectrochemically etched grooves and the concentration of KCl in the electrolyte. Figure 10 shows the SEMs of the cross-section of the V-grooves etched in the (100) GaAs with doping density of $5 \times 10^{17}/cm^3$. The variation of interior angle with KCl concentration is summarized in Table 1, which divides the results into four ranges. When the experiments at each concentration were repeated five times, 80% of the samples fit into these four categories. In addition to the change in the interior angles, as the concentration of KCl was increased the walls of the etched grooves became noticeably scalloped with a periodicity of a few tenths micron. This effect is shown in Figure 11.

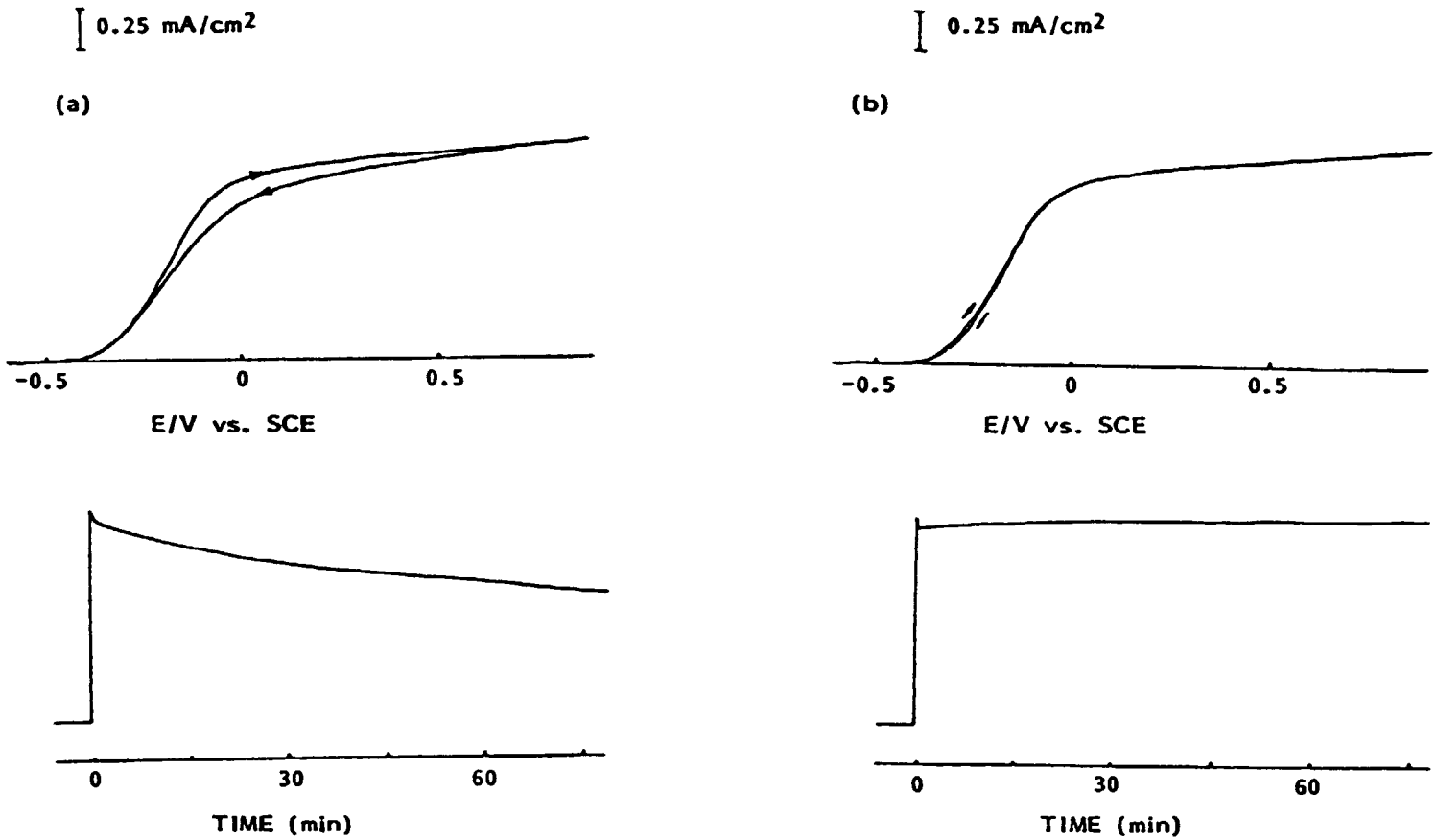

Figure 8. Photocurrent - potential curves for (100) n-GaAs coated with a stripe photoresist mask with a line:space ratio of 2 and a period of 20 μm: a) 1M NaF; b) 0.5M KCl. Sweep rate, 10 mV s^{-1}. Light intensity 30 mW/cm^2.

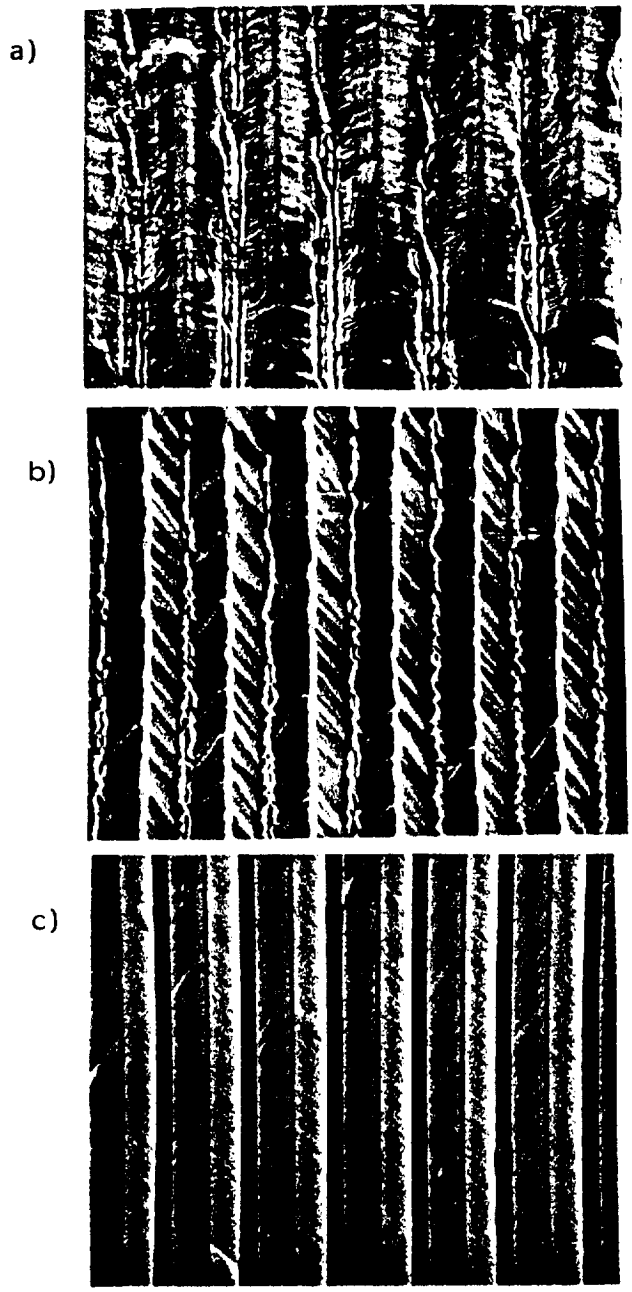

Figure 9. Scanning electron micrographs of V grooves photoelectrochemically etched in (100) n-GaAs along the [01$\bar{1}$] direction, showing effect of electrolyte: a) 1M NaF; b) 0.5M Na_2SO_4; c) 0.5M KCl. Conditions: 0.4V vs. SCE, 30 mW/cm^2.

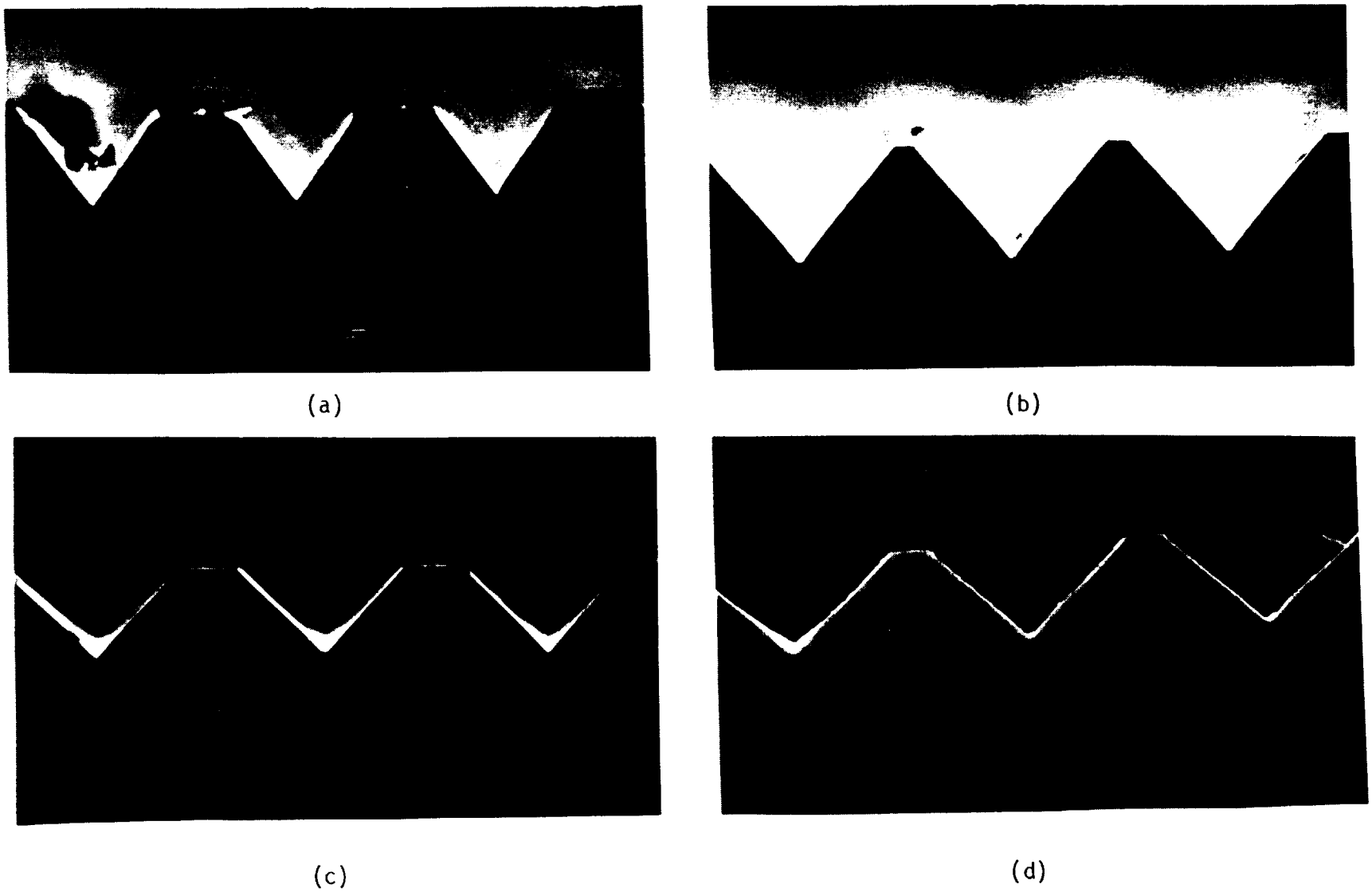

Figure 10. Scanning electron micrographs showing effect of KCl concentration on interior angle of V grooves photoelectrochemically etched in n-GaAs (see Figure 3): a) 0.05M; b) 0.1M; c) 0.5M; d) 1.0M; e) 1.5M; f) 2.5M; g) 3M; h) 4M KCl.

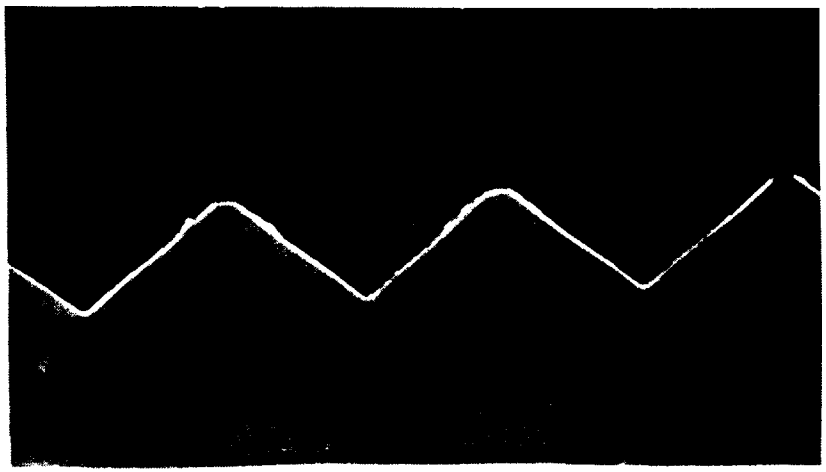

(e)

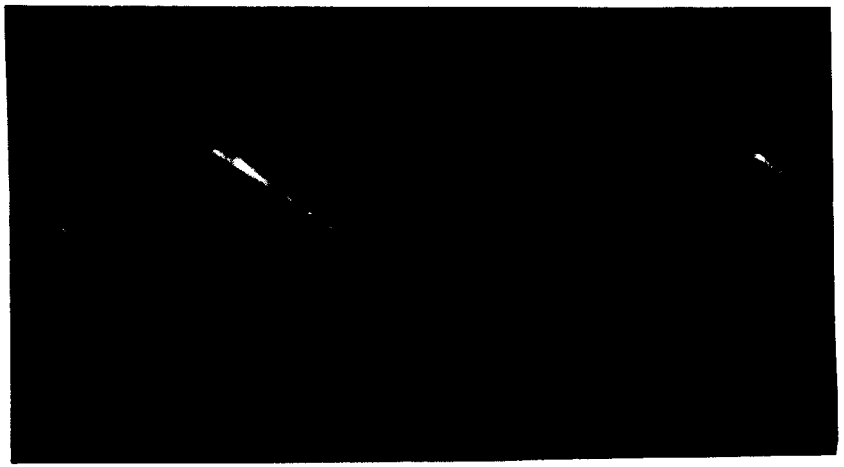

(f)

(g)

(h)

Figure 10 (Continued)

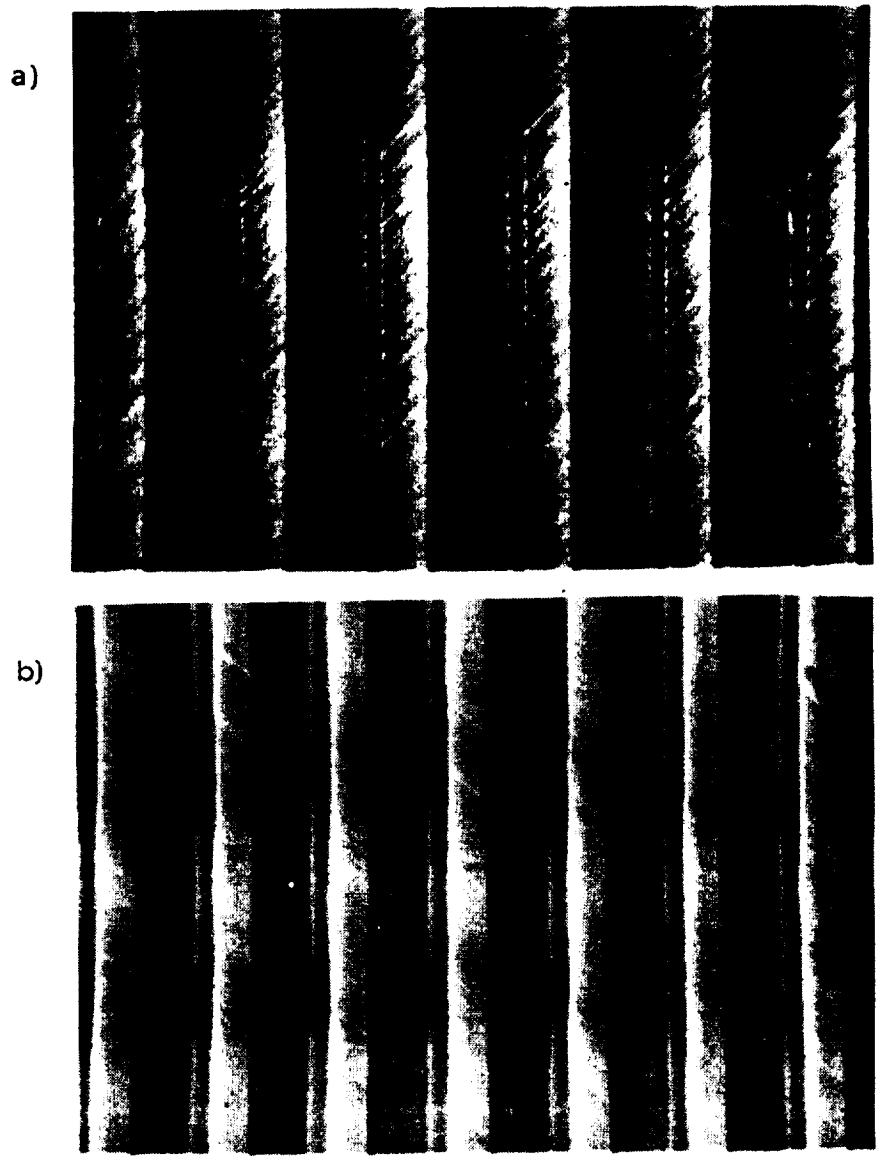

Figure 11. Top view scanning electron micrographs of V-grooves photoelectrochemically etched in n-GaAs in a) 1M KCl and b) 0.05M KCl.

Photoresist Mask Processing Temperature. In order to determine whether surface thermal oxidation affected the etched profiles, the effects of the temperature used to dry the electrode and to hard-bake the photoresist were examined. The other conditions used in the processing were kept constant. The samples were etched in 0.05M KCl at 0.4V vs. SCE under the light intensity 30 mW/cm^2. As seen from Table 2, there was no significant effect of these variables on the interior angle of the V-groove. The photoresist mask prepared in the temperature range 90-140°C appeared sufficiently robust to survive in the KCl electrolyte until the grating was completely formed.

Table 1

Effect of KCl concentration on angle of photoelectrochemically etched V-groove in n-GaAs.

Category	[KCl] Ml^{-1}	Interior Angle (degree)	Crystal Faces
I	0.05 - 0.2	70 - 85	(111)Ga, (332)Ga
II	0.2 - 1.0	90 - 100	(223)Ga, (335)Ga
III	1.0 - 3.0	105 - 115	(112)Ga
IV	> 3.0	120 - 130	(113)Ga

Table 2

Effect of photoresist processing temperature on interior angle of photoelectrochemically etched V-grooves.

Sample	T, Dry °C	T, Hard Bake °C	Interior Angle (Degrees)
1	No	No	85
2	110	110	86
3	No	125	85
4	125	125	83
5	110	140	84
6	140	140	82

All samples were etched in 0.05M KCl at 0.4V (SCE), under a light intensity of 30 W/cm^2.

Applied Bias. The constant potential employed during the photoelectrochemical etching had an effect on the interior angle of V-groove. Taking 0.4V vs. SCE as a reference, increasing the applied bias tended to enhance undercutting and widen the interior angle. Reducing the applied bias suppressed the undercutting. For example, the groove etched at 0.4V vs. SCE in 0.5M KCl had an interior angle of 90°, while angles of 105° and 85° were obtained at applied bias of 1.5V and -0.2V vs. SCE, respectively. A second observation was that the walls of the groove became rougher and pitted as the applied bias was increased.

Illumination Light Intensity. The light intensity affected both the decay of the photocurrent and the undercutting of GaAs beneath the photoresist mask. In 0.05M KCl, for example, the photocurrent was constant with time at 30 mW/cm^2, but decayed after 10 min to 60% and 30% of the original value at intensities of 60 and 180 mW/cm^2, respectively. Figure 12 shows the cross section of the V-grooves etched under 30 and 300 mW/cm^2 illumination in 0.1M KCl. The grooves

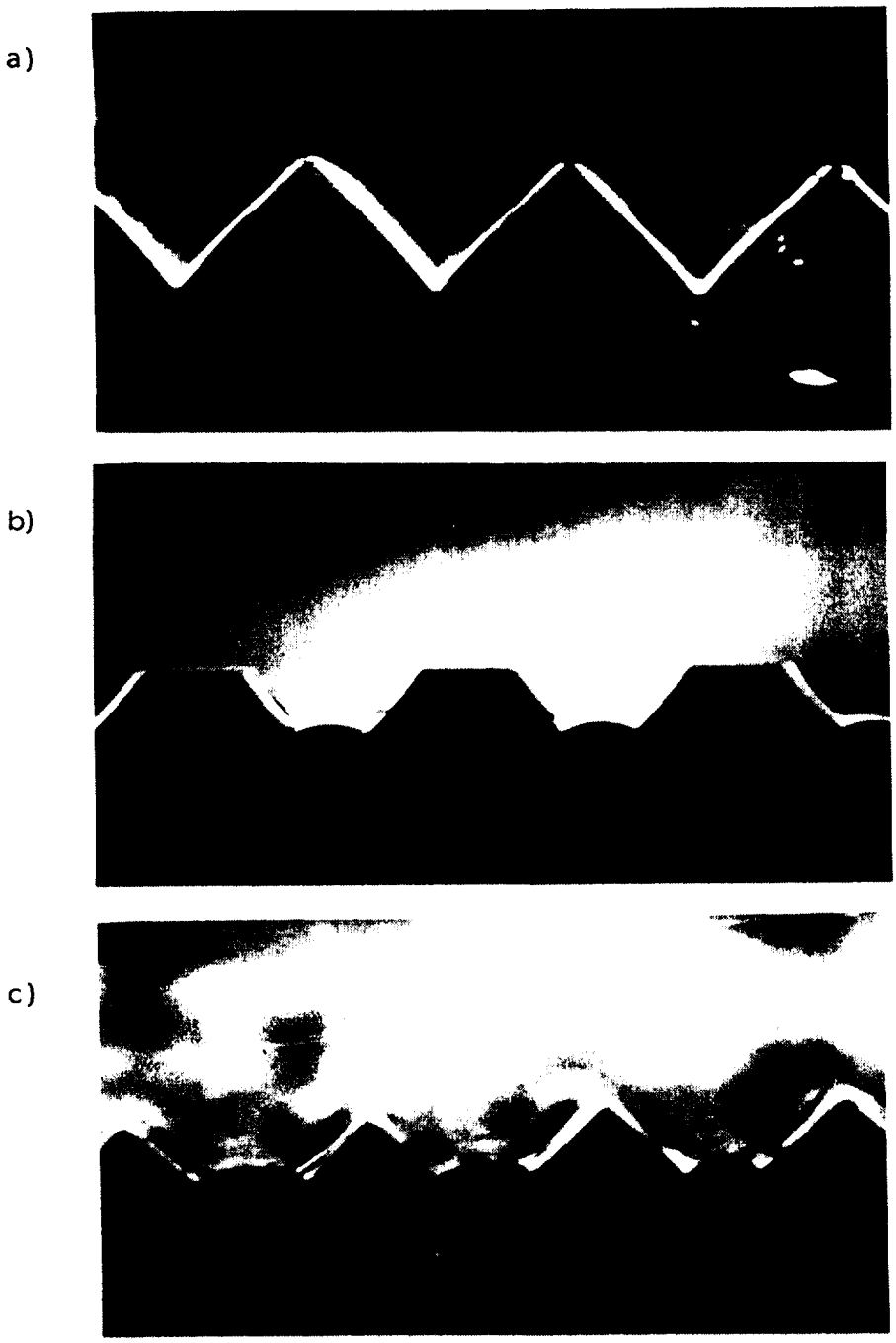

Figure 12. Effect of light intensity on V-groove profiles photoelectrochemically etched in n-GaAs: a) completely formed at 30 mW/cm^2; b) partially formed at 30 mW/cm^2; c) fully formed at 30 mW/cm^2.

formed under 300 mW/cm^2 light intensity have flat bottoms rather than the pointed bottoms which are formed with light intensity of 30 mW/cm^2 (Figure 12a). These flat bottoms formed at an early stage of photoetching (Figure 12b) show that the rate of undercutting was higher than the vertical etching rate. In fact, as the etching progressed (Figure 12c), the depth of the V-grooves did not change significantly indicating that etching was occurring primarily at the Ga-rich plane. The interior angle increased from approximately 85° to 95° on increasing the light intensity.

Doping Density. Figure 13 shows the SEM profiles of the V-grooves etched in GaAs with doping density 6 x 10^{18}/cm^3. Enhanced undercutting was observed in the GaAs with this higher doping density. The pattern etched in 1.5M KCl had shallow, flat bottomed V-grooves with an interior angle of 110° (Figure 13a), similar to that formed in GaAs with doping density of 5 x 10^{17}/cm^3 (Figure 10e). However, rapid horizontal undercutting gave rise to blunt, faceted tops to the grooves at the higher doping density. Narrow flat bottom V-grooves with an interior angle of 95° were produced in 0.5M KCl (Figure 13b). V-grooves with double slopes were obtained on the highest doped samples etched in 0.05M KCl (Figure 13c). The bottom interior angle was approximately 55° while the top angle was 95-100°. None of the photoelectrochemically etched GaAs substrates with lower doping density showed this kind of double sloped V-groove.

Photoelectrochemical Control of Etching Geometry. The results indicate that variables employed in photoelectrochemical etching can be manipulated to control the shape of etched features, here V-grooves in n-GaAs. The evolution of groove geometry is dependent on the relative rates of dissolution along different crystallographic directions. In the present case, a simple V-shape evolves because there is a competition between the progression of dissolution along the [111]Ga (or other Ga-rich face) and the [100] directions. The geometric analysis is shown in Figure 14. Here, the side wall of the V is shown undercutting the mask at a rate A, while the intersection between the (111) and (100) planes is growing out from the mask edge at a rate B. The rates A and B are determined by the rates of etching the Ga rich sidewall (v_{Ga}) and the vertical etching rate v_{100}. We note that undercutting is possibly due to the light transparency of the photoresist mask. The very flat groove faces indicate that attenuation of light passing through the mask is minimal. The following relationships are obvious from Figure 14:

$$v_{Ga} = A \sin\alpha \tag{3}$$

and

$$v_{100} = (A + B)tan\alpha \tag{4}$$

where α is the angle made between the groove face and the (100) surface (54.7° for (111)Ga). Furthermore, a periodic mask will have a minimum space:line ratio necessary to achieve a fully formed groove structure in which the tops and bottoms meet at points. This ratio must ensure that the edges of the groove meet at the bottom before the tops of adjacent grooves form an apex, the latter causing the mask to detach. It is observed that after the point is formed at the bottom, the groove continues to grow by deepening the V through a lateral movement of the Ga-rich plane beneath the mask in the direction of v_{Ga}. The ratio of space to line width may be calculated from equations (3) and (4), viz.:

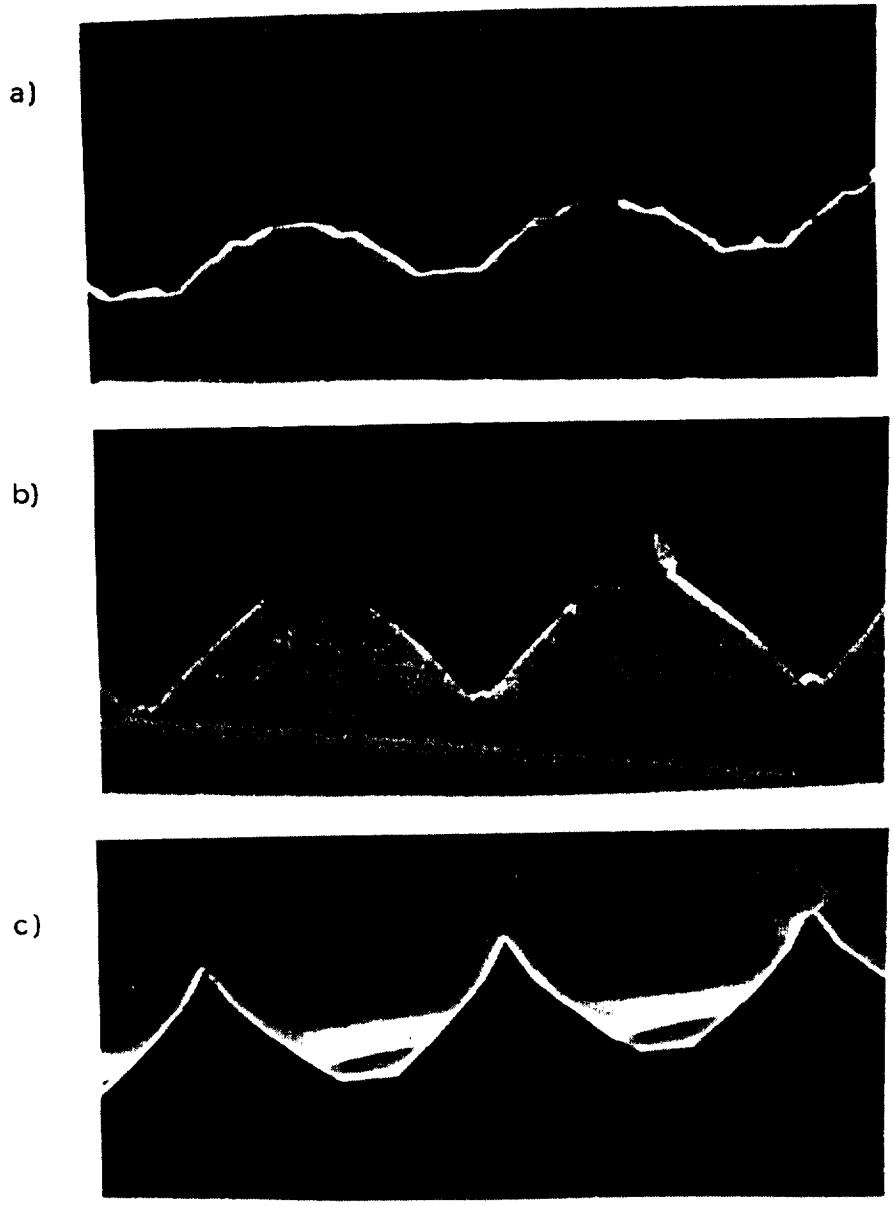

Figure 13. Scanning electron micrographs of V grooves photoelectrochemically etched in (100) n-GaAs along the [01$\bar{1}$] direction, showing effect of increased doping density (6×10^{18} cm^{-3}): a) 1.5M KCl; b) 0.5M KCl; c) 0.05M KCl. Conditions: 0.4V vs. SCE, 30 mW/cm^2.

$$\left(\frac{B}{A}\right) \leq \left(\frac{v_{100}}{v_{Ga}}\right) \cos\alpha - 1 \qquad (5)$$

Examination by SEM of partially etched grooves formed under conditions of Category I, Table 1, gives typical values of the variables in equation (5) as $v_{100}/v_{Ga} = 3.5$, $\alpha = 50°$, and $(B/A) \leq 1.25$. The mask used in these experiments had a ratio of 0.5, so fully formed grating structures were usually obtained.

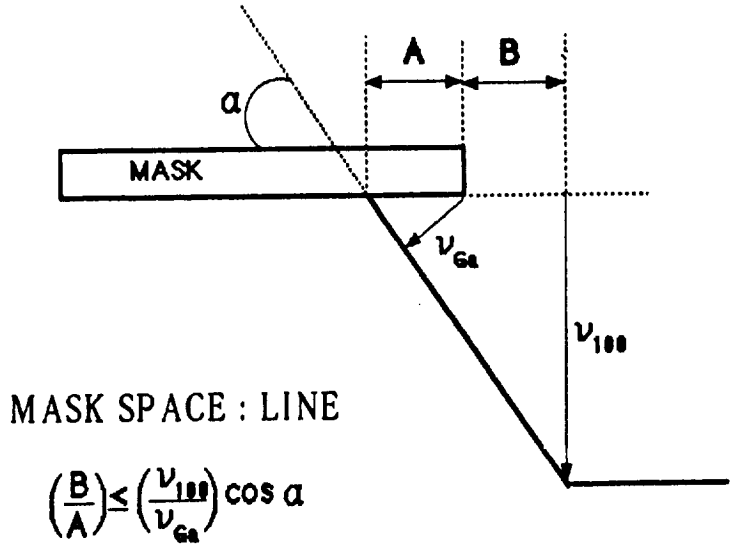

Figure 14. Cross-sectional diagram through (110) plane showing mask undercutting and photoelectrochemical etching rate vectors.

Exceptions to full development of the gratings are shown in Figures 9a and b, for NaF and Na_2SO_4 electrolytes, in Figure 12c for grooves formed under high light intensities, and in Figure 13 for high GaAs doping densities. In these cases, the apex of the grooves formed before their bottoms met. This behavior indicates that (B/A) = 0.5 is too large under these conditions. Fluoride gives rise to passivation, apparently having the effect of decreasing v_{100}/v_{Ga}. Similarly, high light intensity tends to drive etching in the (100) direction into saturation, thus also decreasing v_{100}/v_{Ga}. Saturation may be due to the development of diffusion gradients in the volume space beneath the mask. High doping density is seen primarily to give rise to irregular profiles, rate minima appearing for multiple Ga-rich faces. The cause of this effect is not yet understood, but may relate to diminished spreading of holes at the surface which characterizes increased doping levels.

Etching Chemistry. Photogenerated holes are driven to the GaAs/electrolyte interface and initiate photodissolution of GaAs under illumination with light of a photon energy equal to or higher than the band gap of GaAs (1.42 eV). When using a transparent mask to define the pattern, as is the case here, the light will provide holes at all of the semiconductor/electrolyte interfaces, including those which open up beneath the mask. This etching process is entirely analogous to the case of hole injection by oxidizing chemical etchants [9], so it is not surprising that the crystallographic orientations of the etched features are similar in the two cases. In the potential range over which

the photocurrent is independent of the potential, the magnitude of the photocurrent is proportional to light intensity (analogous to the oxidizing strength of a chemical etchant), and the photoelectrochemical etching is governed by the photon flux.

In a purely aqueous medium, the Ga(III) and As(III) oxidation products would be comprised of the hydrous oxides and oxy-anions/cations [10]. Amphoteric Ga_2O_3 and $Ga(OH)_3$ are only sparingly soluble in H_2O at pH 7, with the major ion in a saturated solution of the hydroxide being GaO^+ (1.5×10^{-7}M). Neutral solutions are near the minimum of the pH-solubility diagram for these species. In contrast, As_2O_3 is relatively soluble in H_2O, with the major soluble species at pH 7 being $HAsO_2$. Thus, it is likely that a contributing factor to the emergence of the Ga-rich faces in photoelectrochemical etching is the low solubility of Ga oxidation products. On the other hand, $GaCl_3$ is more soluble in H_2O than the oxide, forming a series of oxychloride ionic complexes in solution. As(III) does not form chloro-complexes in H_2O, however, so Cl^- would be expected to exert its effect primarily on the kinetics of Ga(III) dissolution. GaF_3 is highly soluble in H_2O, but is insoluble in solutions containing excess NaF, precipitating as $NaF:GaF_3 \geq 8:1$ [11], possibly explaining the passivation observed in NaF-containing electrolytes.

It is also likely that Cl^- participates in the electrodissolution of Ga surface sites via specific adsorption. A simplistic yet useful model of the (111)Ga surface is that Ga atoms are bonded to three As atoms below the surface, and an empty sp^3 hybrid orbital is available for complexation. Of the three anions investigated, Cl^- is adsorbed most strongly onto Ga metal electrodes [12], and a similar preference might be expected for the (111)Ga surface. Halide anion adsorption has been suggested by Kohl et al. to mediate the photoanodic dissolution of n-InP and n-GaAs in aqueous HCl and HBr [13]. These authors also noted that the fluoride anion, being nonpolarizable, should only form solution complexes and not participate as a photodissolution intermediate. Gerischer [14] proposed that the photodissolution of a III-V semiconductor is initiated by nucleophilic attack by an anion with a photogenerated hole:

$$GaAs + Cl^- + h^+ \rightarrow Ga - Cl + As \qquad (6)$$

A higher dissolution rate, therefore, can be expected with an increase in Cl^- concentration. If the Ga dissolution rate is enhanced to such a degree that it becomes comparable to the As dissolution rate, the etching of GaAs will become isotropic. For example, Shaw [15] reported that the (111)Ga plane is revealed on chemical etching of GaAs in 0.87M H_2O_2 solutions with 0.27M HCl, but the etching becomes completely isotropic, with rounded profiles, with 10.6M HCl. The Cl^- adsorption mechanism is also consistent with the effect of bias on the interior angle of the V-groove. Surface states at the GaAs/electrolyte interface will become more positively charged with increased anodic polarization, giving rise to increased adsorption by Cl^-.

The V-grooves formed by anisotropic etching result from the reactivity differences of the surface atoms and can be produced at (100) faces only along the $[01\bar{1}]$ direction. Possible Ga-rich faces and their interior angles are as follows: (111)-70°, (332)-80°, (223)-90°, (335)-95°, (112)-110°, (113)-130°, and (114)-142°. The faces that are observed appear to represent free energy minima for any given set of conditions. Significantly, a (332)Ga plane is revealed at intermediate acid concentrations in the work of Shaw [15]. All of these high index surfaces may be constructed from regular progressions of steps added to fundamental (111)Ga face. They can be visualized as linear combinations of the fundamental {111}, {110} and {100} faces in various proportions. In chemical etching of V-groove structures, higher concentrations of oxidant frequently correspond to higher

interior angles and increased mask undercutting. Scalloping of the side walls observed at high [Cl^-] (Figure 13) is also indicative of the stability of higher order Ga-rich planes. A similar effect is observed when etching groove profiles in GaAs using Br_2/MeOH, with higher Br_2 concentrations giving rise to striations caused by the exposure of {332}Ga planes. It is noteworthy that increasing the oxidation rate by increasing the light intensity up to the maximum tested does not significantly change the groove angle, which is apparently set by the electrolyte composition.

The following model for photoelectrochemical etching is consistent with the results. Holes produced at the (100) surface selectively oxidize and dissolve As due to reduced solubility of Ga(III). The Ga-rich face that is exposed continues to develop at its intersection with the (100) plane and at the mask\GaAs\electrolyte interface due to this kinetic preference. The acidic Ga surface possibly becomes more attractive to holes when complexed with an electron donor such as Cl^-. This would have the effect of reducing the difference in capture cross sections between the two sites and increasing the step frequency and hence the As content of the exposed face, resulting in an increased interior angle. Once the Ga-rich face is established, its rate vector will be reduced geometrically since the face is not normal to the photon flux, viz. $v_{Ga} \leq v_{100} \cos \alpha$. However, the "cosine factor" is not sufficient to explain the observed v_{Ga}, which are typically at least two times lower. We and others have noted previously that the quantum yields for photoelectrochemical etching of (111)A, (111)B and (100) GaAs and InP do not differ greatly in the photon-limited potential region and can be close to unity [2,12]. The additional attenuation of v_{Ga} may indicate a reduced quantum yield for etching the Ga-rich face with continued etching due to gradual passivation or to positive charging of the surface oxide.

3.2 Photoresist Processing: Dip vs. Spin Coating

The very strict requirements of uniformity for Echelle gratings necessitates a highly uniform photoresist coating process. This step was investigated in some detail. In particular, flow controlled dip coating was investigated as an alternative method to spinning for coating semiconductor surfaces. During flow controlled dip coating, instead of pulling the samples out of the liquid, the liquid is drained at a particular flow rate. This allows the sample to remain motionless while the characteristics of the film are controlled by the rate of the flow.

Spin Coating. Before discussing our method of dip coating, it is important to note more carefully some of the advantages and disadvantages of spin coating. Of primary importance is the uniformity of the photoresist film and the latitude or degree of reproducibility with which a desired film thickness can be produced. A good commercial spin coating device can produce a uniformity in film thickness of 100Å or less (to three standard deviations) with a wafer to wafer deviation of 120Å (to three standard deviations). This can be accomplished over a six inch wafer [16,17]. The primary disadvantage of spin coating is the production of radial patterns in the photoresist film. Even with the advancement of VLSI, minimizing these striations is a continued problem. The striations do not occur when dip coating. After some preliminary experiments, we focused our investigation on whether or not the necessary degree of film thickness uniformity and latitude can be achieved by dip coating.

Our experience with spin coating can be used to determine the degree of film thickness uniformity and latitude required for reproduction of the Ronchi pattern on the GaAs crystal surface. For the attempted construction of a diffraction grating with a period of 50 lines/mm and a previously determined optimum line space ratio of 2:1, we need to resolve about 12 or 13 μm lines with about

6 or 7 μm spaces. With the current conditions of light intensity and resist development, it takes about 6 seconds of light exposure to resolve the 2:1 pattern in a 2 μm thick film and 4 seconds to resolve the pattern in a 1.5 μm film. That is, we are cutting through about 0.33 μm of photoresist with each second of exposure.

Overexposure of the photoresist causes loss of definition of the pattern. For spin coated samples, we have observed that an increase in exposure time of only 0.2 seconds will result in some loss of definition, effectively changing our line:space ratio from 2:1 to 1:1. We therefore need to control our film thickness with a corresponding degree of uniformity and latitude. That is, the film thickness deviation must correspond to less than 0.1 seconds of exposure time or 330Å.

An optimum film thickness of 1.5 μm was found when using spin coating. Films that are less than 1.0 μm are highly susceptible to surface induced coating irregularities. A piece of dust or surface defect induces problems in submicron films that do not occur in thicker films. Films thicker than 2.5 μm make it difficult to resolve the 2:1 pattern. When enough light is applied to cut through the photoresist film, it tends to expose the masked areas as well. When fully developed, the pattern (as a function of exposure time) will either fail to be cut through to the GaAs surface or will be completely washed away. Films in the 1.5 to 2.0 μm range yield well resolved 2:1 patterns with little or no surface induced striations.

Dip Coating: Experimental. The dip coating system was constructed from a glass vessel with a Teflon stopcock on the end. The glass vessel contained the photoresist. The substrate was mounted on a Teflon block and suspended in a vertical position inside the glass vessel. The entire dip coating system was isolated from vibrations by working on an optical table with a gas suspension system. Opening the stopcock allowed the liquid to flow, the falling liquid coating the substrate. In order to measure the flow rate, the time required to dip the sample was recorded with a stopwatch, and the amount of liquid flowing out of the system during the dip was measured with a graduated cylinder. After coating, the freshly dipped substrate was allowed to remain suspended inside the chamber in a vertical position for several minutes to allow the top and bottom elements of the film to "dry" evenly. The samples were then placed in an oven for the soft bake procedure. Further processing is done according to the manufacturer's instructions. The photoresist used was Shipley S1400-31. Experiments were conducted by mixing the photoresist with various amounts of Shipley Type A thinner (for details see below).

Surface profilometry was used to measure the film thickness at various locations along the surface, and to determine the uniformity in film thickness. After soft baking the samples, a simple mask was used to reveal a two millimeter strip of bare GaAs on the side of the sample next to a developed photoresist film. The profilometer (Sloan Dektak) was used to measure the film thickness along the length of the sample at two millimeter intervals (± 0.5 mm). At least two but usually three measurements were made at each location and the average is taken as the film thickness. The uncertainty in the distance measurements (±0.5μm) was primarily due to human error in positioning the profilometer needle. The uncertainty in the film thickness measurements is calculated to be ± 200Å. This uncertainty reflects the average of the uncertainties in film thickness determined at each measurement position.

The uncertainty in film thickness at each position was determined by taking the standard deviation of all the measurements made at a given position. The thickness measurements were then graphed as a function of position and fit to a line using regression analysis. In most cases, and especially at higher flow rates, the data fit a line well. The correlation coefficients were typically

over 0.9. We end up with the average film thickness across the width of the film, the standard deviation in film thickness, and the regression coefficient. The regression coefficient provides a measure of the linear differential thickening of the film along the length of the sample. A negative gradient means the film was thicker at the top than at the bottom. With the data reduced, we determine how the average film thickness and the film thickness uniformity depend on key dip coating parameters. These parameters include flow rate, viscosity, and the length of the post dip vapor phase.

Dip Coating Results. Using the above procedure, measurements were made at various flow rates and with various amounts of thinner added to the photoresist.[1] Figure 15 shows the average film thickness versus the flow rate with various amounts of thinner added. We can divide the graph into three main regions: flow rates below 5, flow rates between 5 and 25, and flow rates larger than 25. For flow rates below 5, the film thickness is independent of the amount of thinner used and begins to become independent of the flow rate. A flow rate of 5 to 25 ml/min is in a highly critical region. We see that increasing the flow rate will increase the thickness of the film. Decreasing the amount of thinner will also increase the thickness of the film. Beyond a flow rate of 25 ml/min, the film thickness dependence on flow rate becomes minimal. We also see that the minimum film thickness obtainable is 0.5 μm and the thickest films are about 3.0 μm thick. The 0.5 μm limit is reached when the flow rate is less then 3 or 4 ml/min (independent of the amount of thinner used) or with a resist coat containing 50% thinner (independent of the flow rate). This graph shows the degree to which reproducible photoresist films can be applied by dip coating. It is interesting to note that these curves are highly reproducible (data were collected over a period of weeks and by two independent experimenters) and the curves are quite independent of the incorporated rest period (see below). Also, the measurements of the average film thickness fit onto the graph well even if the film is not very uniform.

Not only do we have to control the film thickness but also the film thickness uniformity. We have determined that a linear differential thickening of the photoresist film along the length of the sample is the most serious type of nonuniformity. Figure 16 shows this gradient as a function of flow rate under various conditions. We see things are not as simple as they were for the average film thickness measurements. The graph showing the effect of the parameters studied on the film thickness gradient is not well understood; other parameters not investigated may also be important. The most careful investigation was done with the 25% thinner 75% photoresist system. In Figure 17, we see a correlation between thickness gradient and flow rate. The gradient becomes minimal at flow rates below 12 ml/min. We also see that this nonuniformity is affected by the incorporation of a five and ten minute rest period (the vertical vapor phase mentioned above) and that this rest period may be critical in producing the desired films.

Other pieces of useful information can be obtained from the same set of data. Figure 18 shows that the thickness gradient is independent of the average thickness. It should be possible to choose any allowable film thickness and still minimize the thickness gradient. Table 3 shows values for one standard deviation in film thickness for several samples. In a few cases, an encouraging deviation of under 500Å is achieved, but in most cases the deviation is 500 to 1000Å.

[1] To allow for comparison and reproduction of this work, flow rates (ml/min) can be converted to drop rates (cm/min) by multiplying the flow rate by 0.06.

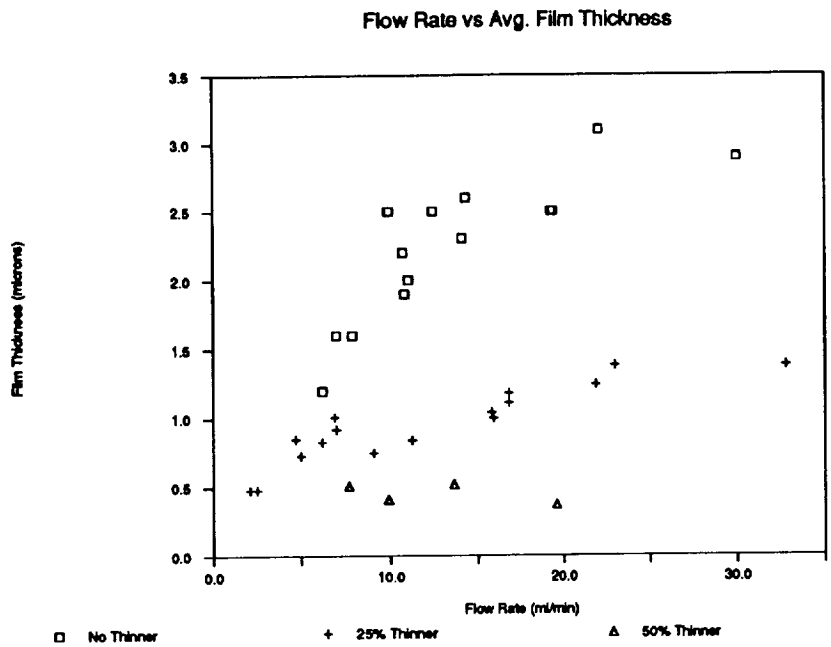

Figure 15. Average thickness as a function of flow rate for several viscosities.

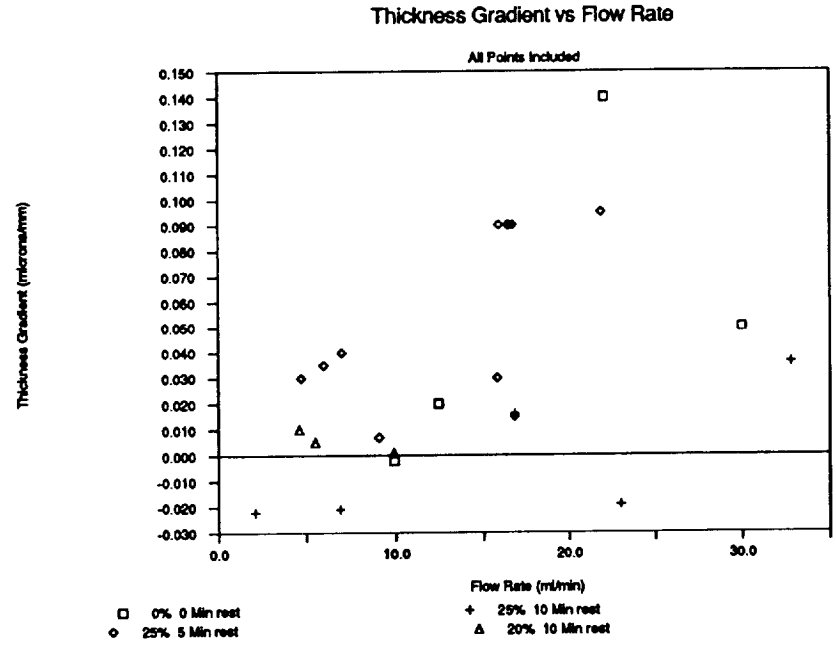

Figure 16. Thickness gradient as a function of flow rate, viscosity and rest period.

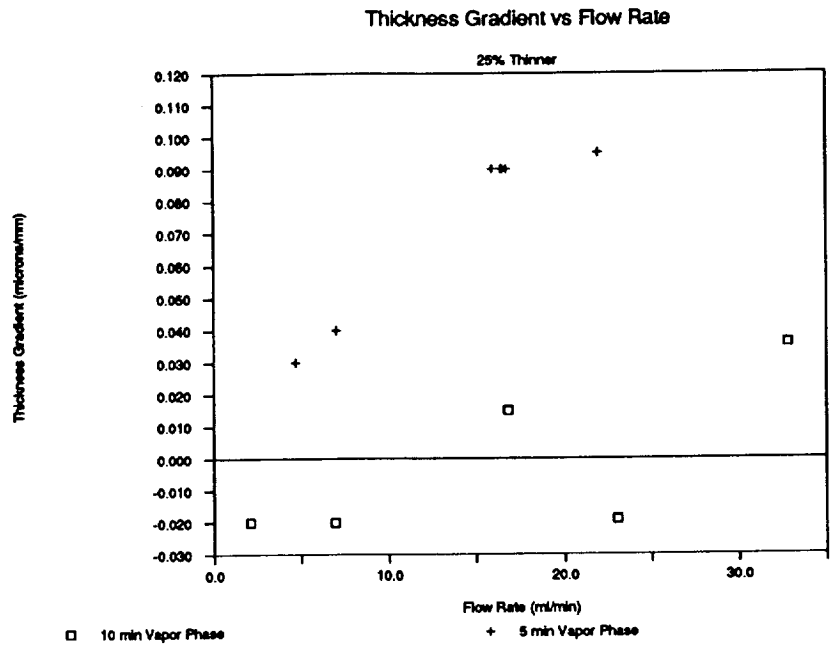

Figure 17. Thickness gradient as a function of flow rate for the 25% thinner system only.

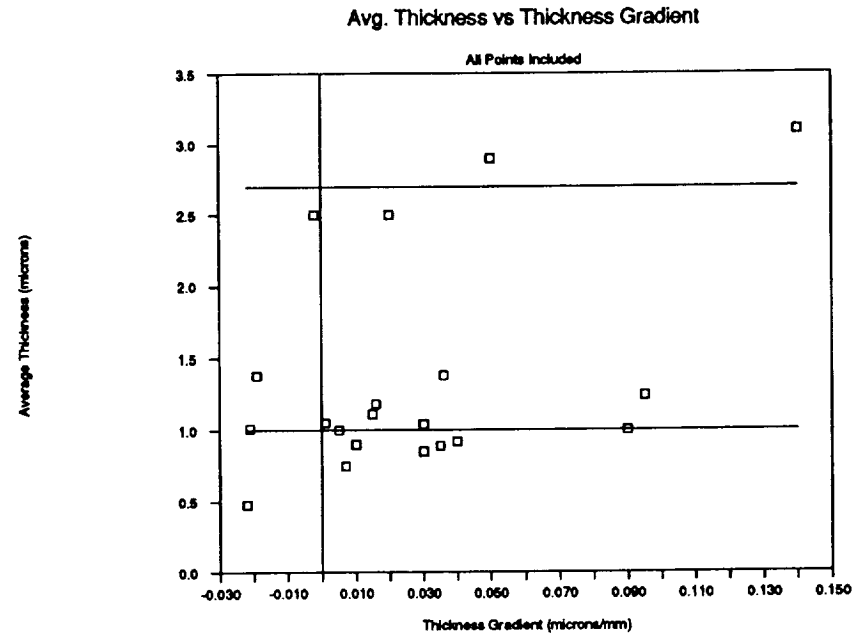

Figure 18. Thickness gradient as a function of average thickness.

Table 3. Representative thickness data showing the deviation in film thickness.

Representative Thickness Data			
Gradient (Å/cm)	Average Thickness (μm)	One Standard Deviation (Å)	Flow Rate (ml/min)
200	2.5	250	9.9
500	1.0	1000	5.5
1000	0.9	900	4.6
1500	1.1	500	16.8
1900	1.4	700	23.0
2000	2.5	930	12.4
2100	1.0	500	6.9
2200	0.5	700	2.1
3600	1.4	1700	32.8
5000	2.9	1800	30.0
9500	1.2	3400	21.9
14000	3.1	4000	22.1

Dip Coating: Discussion of Results. Let us explain what we think is happening during the dip coating procedure. First, consider the line of contact between the photoresist liquid and the photoresist film. This is the line where the liquid and gas interface touches the GaAs sample surface. While the liquid drains, the surface tension at this interface pulls the deposited photoresist film back into the liquid photoresist decreasing the film thickness. When the substrate is dipped quickly, the liquid has less time to pull the photoresist off the substrate surface. This produces a thicker film. This interesting phenomenon can be demonstrated at home by dipping one butter knife quickly and another slowly into some vegetable oil. The quickly dipped knife will have a thicker film. This is also what the average film thickness curves show. As the liquid level drops, the photoresist film on the substrate remains wet and falls under the force of gravity. As the film falls, it drys and continues to fall until a type of frictional force between the solid and liquid interface slows the progression of the liquid.

Consider a differential volume element of liquid at some position along the length of the sample. Liquid is flowing in at the top; at the same time, liquid is flowing out of the bottom and the solvent is evaporating. A differential element toward the top of the sample has been exposed to air for two or three minutes before the dropping liquid exposes a differential element toward the bottom of the sample. After a time that is long compared to the drop time, the states of the differential elements at the top of the sample and those at the bottom of the sample will converge to an evolving state of similar time dependence. This is why a ten or fifteen minute vapor phase is incorporated.

Similarly, this explains an increase in the film thickness gradient with the liquid drop rate. If the liquid drops quickly, thick wet differential fluid elements are produced that evolve dramatically with time. If the liquid falls slowly, the differential fluid element directly above the liquid level may dry before the neighboring fluid element below is exposed to air. In the second case, no evolving fluid elements would be produced. Unfortunately, this would produce a film that is too thin (about 0.5 μm). We now know that a slow liquid drop rate and a vertical vapor phase are important in producing uniform photoresist films.

We may now ask, how can we produce the desired film of 1.5 μm with a minimal thickness gradient? Referring to Figure 14, we see flow rates below 5 ml/min cannot be used because the films are too thin. It would also be desirable to avoid the 5 to 20 ml/min region because of the highly critical flow rate dependence. Ideally, one would like to work on the flat part of the curves and simply control the film thickness by adjusting the amount of thinner added to the resist. This, however, fails because of the thickness gradient (see Figure 16). The gradient measurements indicate that for a film with any degree of uniformity one must use a flow rate below 20 ml/min. In reality, the only highly uniform films made were produced with a flow rate close to 10 ml/min. This, however, puts us on the highly critical portion of the average thickness versus flow rate curve. Unfortunately, this is the only area with any possible chance of producing the required films.

The best films are produced with photoresist containing 10 or 15% thinner, at a flow rate of 10 ml/min, and with the incorporation of at least a 10 minute vapor phase. A flow rate of exactly 10 ml/min, however, may produce a wafer-to-wafer deviation in film thickness as large as 1000Å. It may be possible to coat a large enough number of wafers to produce a few with the target film thickness, but then the film thickness on each single wafer may deviate unacceptably. As the final chart shows this deviation can be as large as 500 to 1000Å or two to three times an acceptable level.

Conclusion. From the experiments conducted, we see that it is very difficult to produce dip coated photoresist films that can compete with those of spin coating. In order to eliminate the problem of linear thickening, one must operate in a flow rate regime where the average film thickness is difficult to control. This produces a critical loss of latitude. If the desired latitude could be met by better controlling the liquid drop rate, there is still a lack of uniformity that is five to ten times that of spin coating. It should also be noted that the dip coating seems to be more dependent on the quality of the surface preparation. That is, surface induced striations that occur when dip coating do not appear when spinning. A detailed analysis of this situation was not conducted. There are system modifications that were not tried. The most important might be a post dip horizontal drying period. Allowing the samples to dry in a horizontal position before the soft bake procedure may allow the photoresist film to level before drying.

EIC has recently purchased a commercial spin coating system. This system can coat larger samples with higher quality than is currently possible with our home made spin coater or dip coater. Experiments that are difficult to do on our home made spin coater will be easy on the new one. These experiments include varying the spin speed, spin time, acceleration, deceleration and perhaps even the rate of exhausting of the spin bowl. For example, the spin time may affect the induced radial striations. Since the striations may be due to premature drying of the photoresist in the spin bowl [16], decreasing the spin time may help eliminate this problem. The pre-softbake horizontal drying procedure suggested above for the dip coating operation may also be tried with the spin coating to minimize the occurrence of the radial patterns. With this information, it was decided to discontinue research on the dip coating system in favor of using the new commercial spin coater.

The new spin coater was used to make the photoresist films for the final gratings. Time did not allow for experimentation so previously determined spin coating parameters were used with modifications made out of necessity. The previously used spin time of 45 seconds was lowered to 25 seconds, and the samples were allowed to dry for 15 minutes at room temperature before soft baking. These modifications were made with the hope of eliminating the radial patterns. The spin speed was 5000 RPM. A well resolved 2:1 pattern was achieved but the radial patterns persisted. This was the method used for the final grating fabrication.

3.3 Surface Preparation of GaAs

Background. Optical devices such as diffraction gratings require flat mirror surfaces. Etching perfectly smooth grating walls requires a surface with a highly perfect crystal microstructure. This is because damage not apparent after polishing can be revealed by etching. Flat surfaces can be achieved by mechanical polishing with abrasives, while chemical etches can be used to produce surfaces that clearly reveal the crystal microstructure. Unfortunately, optimizing both characteristics is mutually exclusive. Chemomechanical polishing is used to exploit the advantages of both types of polishing. During chemomechanical polishing, an etchant is used to attack or oxidize the crystal surface, while small particles or the polishing pad removed the affected surface layer.

Most polishing procedures consist of three steps: lapping, rough polishing, and fine polishing. The lapping step accomplishes two things: it shapes the material (in our case makes it flat) and removes the layer of damage caused by previous process steps including slicing and rough grinding. The rough polishing step is used to remove the damage caused by lapping. It can be thought of as a material removal step but not as a shaping step. Once the sample is made flat by lapping, polishing will only upset the flatness. Maintaining the flatness depends on minimizing the time required to polish the samples. Final polishing is done to remove the scratches caused by rough polishing.

In the past, polishing our GaAs samples consisted of lapping with 600 grit silicon carbide paper, then mechanically polishing the samples with a series of alumina steps ranging in particle size from 5 μm to 0.05 μm. Chemomechanical polishing was used as a final step. The resulting samples had a fine surface microstructure but inadequate flatness. Many of the process conditions were analyzed to determine the effect on sample flatness and quality. In addition, several new polishing materials were tested to see if they would improve the results of our surface preparation procedure. The resulting procedure produces flatter samples with a minimal amount of microstructural imperfection.

The previous method of polishing is summarized in Table 4. The fine grinding steps are done with Buehler Carbimet SiC paper, the alumina steps on a fine polishing cloth (Alpha Lap, Optical Manufacturers Inc.), and the chemomechanical polishing on a foamed polyurethane pad with a buffed surface (GP 430 Optical Manufacturers Inc.). The chemomechanical slurry is a mixture of bleach, water, and a colloidal silica (Nalco 2360, Rodel Manufacturers Inc.) mixed, according to the manufacturer's instructions, 1:1:10 slurry:bleach:water. The times noted are roughly correct but varied as much as an hour from run to run.

Table 4. An outline of the previous method of polishing GaAs at EIC Laboratories.

Previous Method of Polishing GaAs		
Polishing Step	Process Condition	Process Time
Epoxy Removal	120 grit paper	Varies
Lapping	600 grit paper	30 min
Rough Polishing	5 μm alumina 1 μm alumina	3 hrs 3 hrs
Final Polishing	0.3 μm alumina 0.05 μm alumina	2 hrs 3 hrs
Chemomechanical Polishing	0.06 μm Silica Slurry and Bleach	3 hrs

The first thing to note is that 120 grit paper is used to remove the epoxy from the sample surface. The large size of these hard and jagged particles will cause deep layers of damage in the soft gallium arsenide. This increases the polishing times required for adequate surface preparation and results in a less flat wafer. Another problem with the process is the prolonged alumina polishing steps. By minimizing or eliminating unnecessary steps, a flatter wafer will result.

Experimental Procedure. The polisher was an Ecomet III polisher/grinder with a Whirlimet polishing attachment; both devices were manufactured by Buehler. The Whirlimet slowly rotates the wafer as it is being polished by the rotating pad. The wafer was held against the pad with a slight amount of pressure (about 1/2 psi). A pump was used to drip the suspended alumina or silica slurry onto the pad at a constant rate. The experiments consisted of trying alternative polishing processes and materials and analyzing their effect on wafer surface quality and flatness.

The surfaces were analyzed for flatness by comparing their laser reflections (442 nm or 632 nm) to those of an optical flat. This was done using large and small angles af incidence. By using large incidence angles and observing the reflection at large distances, an imperfectly flat wafer will produce an astigmatism. The degree of the astigmatism can be used as a measure of sample flatness. The surfaces were examined using an optical metallograph and a scanning electron microscope. Because a sample that appears perfect after polishing may still have a damaged microstructure, the samples were etched in our photoelectrochemical cell. The results of this are shown in Figures 19 and 20. The photoelectrochemical process was used, as opposed to other etches, because this would most accurately reflect the effect new surface preparation conditions have on the quality of the diffraction gratings.

Epoxy Removal and Lapping. The use of 120 grit Carbimet paper to remove the epoxy was unsatisfactory. It can create a damaged layer in the sample hundreds of microns deep. Three other methods were tried: the use of 600 grit paper, the use of 20 μm alumina on a cast iron lapping wheel, and the use of 20 micron alumina on a lapping pad (Delta 8100, Optical Manufacturers Inc.). The last two methods produced the best sample surfaces but took over 16 hours to accomplish. The 600 grit paper worked well and only took a couple of hours. If enough water is used so that the samples are almost hydroplaning, the 600 grit paper can be used with little damage to the wafers.

Upon meeting with NASA's polishing group, we decided to try a new lapping method to replace the 600 grit paper previously used (Table 5). Lapping was done on a spiral grooved cast iron wheel, with 20 μm alumina, and water as a lubricant. Lapping damage in GaAs has been found to occur at as large a depth as three times the particle size [18]; therefore, the 20 μm alumina was replaced with 5 μm alumina. The use of water as a lubricant damages the flatness of the cast iron wheel and was replaced with an oil (Buehler Polishing Oil). The oil not only preserves the flatness of the wheel but, as the lapping operation continued, also coats the GaAs surface. This may produce a protective layer decreasing the effective size of the lapping particles. It was found through experiments and the material removal rate studies explained below that the optimum lapping time is four hours.

Concave/Convex Surfaces. When a polishing attachment is used to hold and rotate the samples on the pad, the edges of the sample turn more quickly than the center. This causes a faster rate of material removal toward the edges of the sample and a convexity known as "pillowing" results [19]. At a constant wheel speed, this is a function of grit size and polishing time. A study was conducted with each of the grit sizes to determine when noticeable pillowing occurs. The results are shown below. With this information, we can determine how long we can polish at a certain grit size and still maintain sample flatness. Notice that pillowing occurs more quickly for smaller size particles. Perhaps this is due to a decrease in the effective wheel speed, i.e., a slower material removal rate. This makes more pronounced the effect of the samples turning in the polishing attachment.

During the chemomechanical polishing operation the NaOCl etches the GaAs surface but not the epoxy the sample is mounted in. This results in an increased material removal rate toward the center of the sample we call cupping. With chemomechanical polishing on a fine polishing pad, this occurs after about three hours of polishing. One method of creating a flat sample would be to pit the pillowing against the cupping. More often than not, however, this results in a wavy fun-house mirror surface. The best method is to use the information obtained and keep the polishing times to a minimum. If necessary, increase the wheel speed to minimize the pillowing effect.

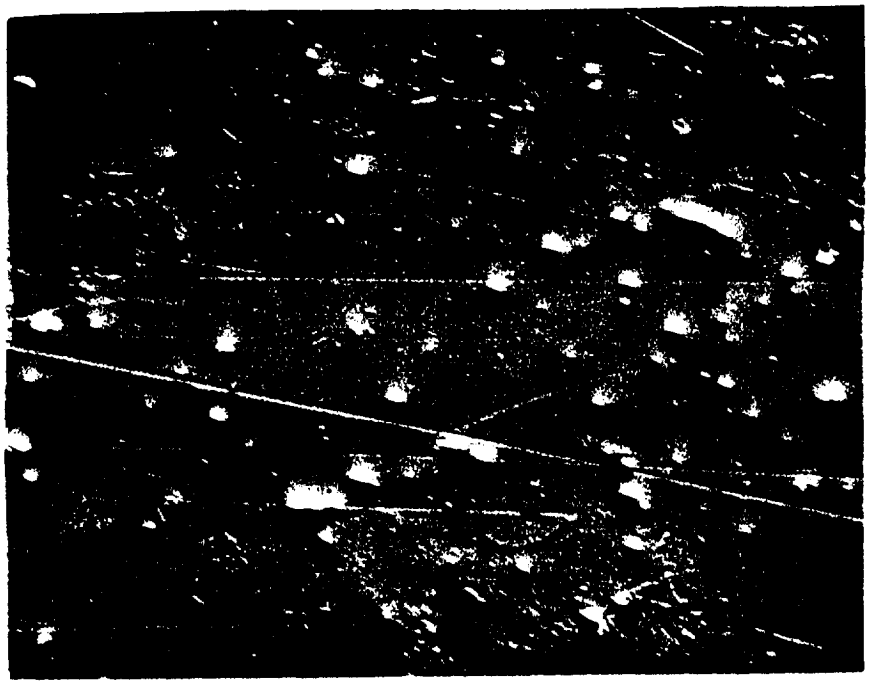

Figure 19. An SEM micrograph of a sample showing material defects (etch pits) and polishing defects (scratches) magnified 160X. The defects were revealed by PEC etching.

Figure 20. An SEM micrograph of a sample showing material defects, but no polishing defects, magnified 160X.

Table 5. The minimum length of polishing time before visible pillowing or cupping appears.

Length of Polishing Operation Before Noticeable Pillowing and Cupping Occurs	
Polishing Step	Minimum Time
5 μm alumina	10 hrs
1 μm alumina	3 hrs
0.3 μm alumina	1 hr
0.05 μm alumina	< 1 hr
chemomechanical	3 hrs

Material Removal Rate. Experiments were conducted to determine the material removal rate for the lapping operation, the 5 μm polishing step, and the chemomechanical polishing operation. This information is useful for approximating the minimum time required to remove the damage caused by previous polishing steps. Most of the experiments consist of simply recording the time required to polish off unusable gratings. Other experiments were conducted using optolithographic techniques and our photoelectrochemical cell to etch squares of known depths into the samples. The time required to polish off the squares is recorded and the material removal rate determined. For the lapping operation, defective samples are used and the time required to lap through the entire length of the sample is recorded. The measurements made using the three different methods agree.

The material removal rate for the lapping operation is 45 ± 5 μm/hr. The material removal rate for both the 5 μm alumina polishing step and the chemomechanical polishing step is about 3 ± 1 μm/hr. While the material removal rates are the same for the both alumina and chemomechanical polishing, the effect of each process is very different. Alumina polishing will tend to hide a damaged microstructure while chemomechanical polishing, because it is primarily an etch, will tend to accent damage. We see that the effects of using the smaller size alumina particles is minimal, since the material removal rate for the chemomechanical polishing is comparatively high. The material removal rate is probably dependent on flow rate and wheel speed. Both of these parameters were not investigated.

Comparison of Three Polishing Methods. Using the above information as a guide, a comparison was made of the methods that produce the flattest wafers. In all cases, 600 grit paper is used to remove the epoxy from the sample surfaces and the four hour lapping procedure discussed above is employed. Method one is simply to polish the samples chemomechanically for two hours after lapping. Method two is to polish the samples chemomechanically for about two hours, next

polish with 5 μm alumina for three hours, and finally polish the samples again chemomechanically for about an hour. The third method was to polish chemomechanically with a stock removal pad (GP IV, Optical Manufactures, Inc.) for two or three hours and then polish chemomechanically with a fine polishing pad for one hour. Each method yields good wafers and bad wafers but the third method produces good wafers more consistently. Fine chemomechanical polishing directly after lapping tends to result in wafers with 5 μm scratches as a result of the lapping operation. Incorporating the 5 μm alumina step causes its own damage that requires over three hours of final chemomechanical polishing to remove. The third method yields wafers with fewer surface defects but some cupping. While the wafers produced using the third method were pretty good a slight amount of orange peeling is present. Attempts to remove the orange peel with 0.3 μm alumina were unsuccessful.

In conclusion, the best GaAs wafers produced on EIC's polishing equipment are made by lapping on a cast iron wheel followed by a two step chemomechanical polishing process. While the wafers are flat and reveal the microstructure well, they also have an orange peel look to them. The effect of this orange peel on the quality of the diffraction gratings is not clear but seems minimal. This method was employed for the final grating construction.

4.0 FINAL GRATING FABRICATION

A final set of gratings was fabricated at the end of the program. A mask ruled at NASA was incorporated into our grating fabrication process with success. The checkerboard pattern associated with the previous mask is no longer present. Time and lack of material did not allow for the construction of enough samples to determine the effect the elimination of the checkerboard pattern will have on the scattering properties of the diffraction gratings. Great care was taken in incorporating the mask into our PEC process. This was difficult because unless the mask makes intimate contact with the sample surface, interference patterns in the photoresist result. The final gratings were constructed using the new mask. The following experimental parameters used to photoelectrochemically etch the gratings are contained in Table 6.

The improved polishing method, the NASA ruled mask, and new spin coating machine were used to construct several diffraction gratings. The gratings had smooth walls and pointed tops and bottoms. Unfortunately, there still remain etch pits. The SEM's in Figures 21 to 23 show areas of the gratings at various magnifications. The etch pits are shown clearly at the highest magnification. Although improvements have been made in increasing the size and quality of GaAs wafers over the past two years (EPD < 10,000/cm^2 for two inch wafers), they are still not of the high quality required for diffraction gratings. Rough experiments done with our lasers suggest that most of the stray light scattering accompanying these gratings is due to etch pits. Perhaps in the future, material growth improvements will allow the fabrication of high quality diffraction gratings in GaAs using our PEC process. In the immediate future we will begin work with silicon, in which large wafers can be grown with near zero EPD.

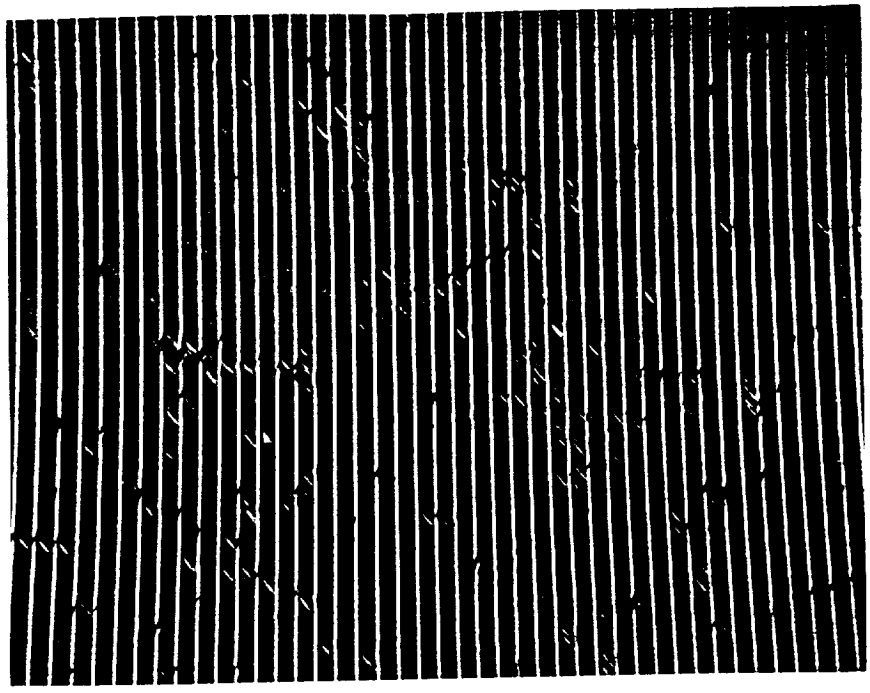

Figure 21. An SEM micrograph of a GaAs grating magnified 140X showing material defects.

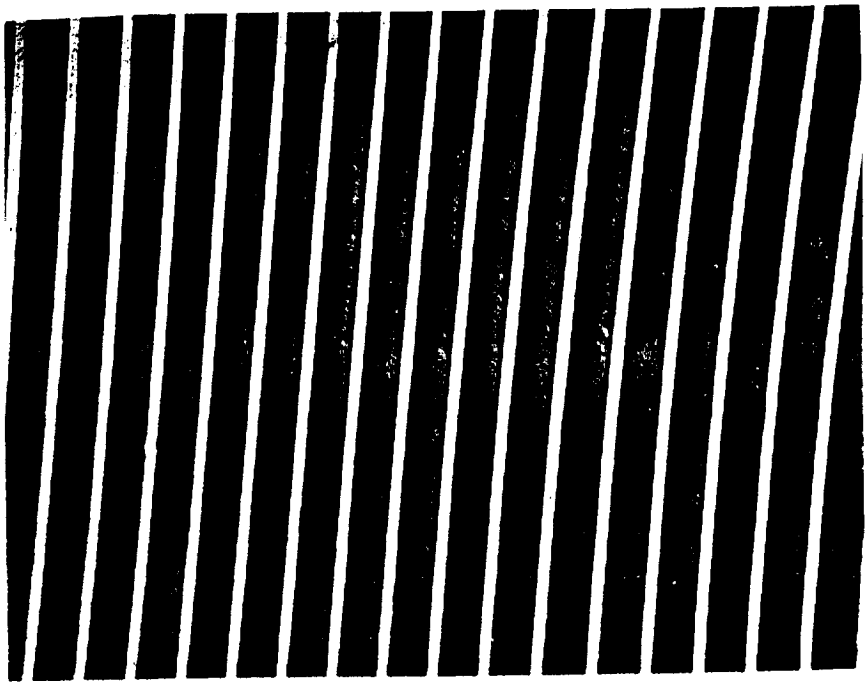

Figure 22. An SEM micrograph of a GaAs diffraction grating magnified 300X. Some areas of the grating are defect free.

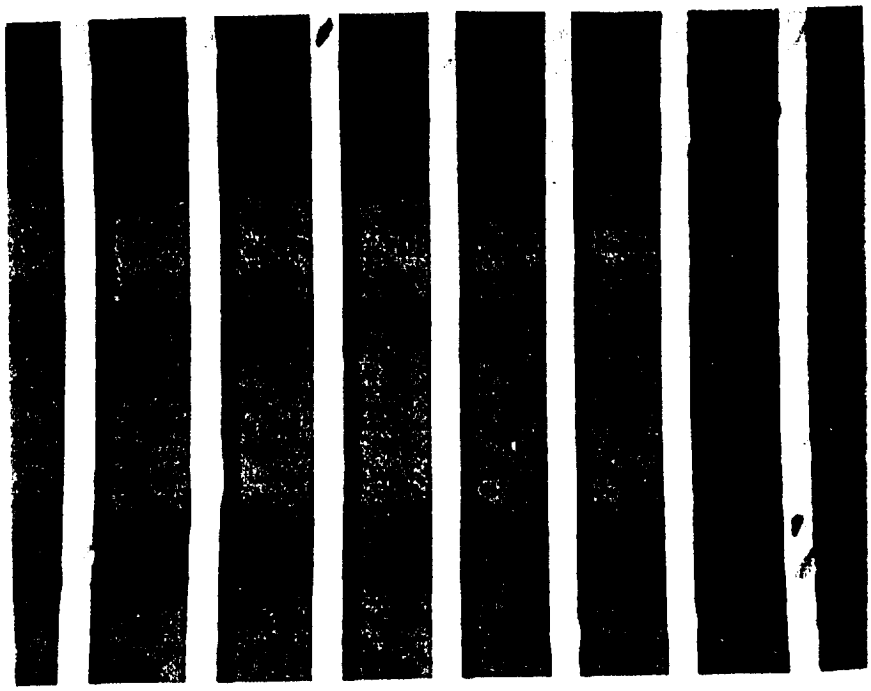

Figure 23. An SEM micrograph of a GaAs grating magnified 820X. Etch pits are clearly visible.

Table 6

Final GaAs Grating Parameters

GaAs Material Parameters	
Grating Material	n-type GaAs, Si doped, (100) and (100-18) orientation.
Doping Density	$1X10^{17}$-$6X10^{18}/cm^2$ (100), $5X10^{17}/cm^2$ (100-18).
Surface Preparation	Cast iron lapping, 5μ Al_2O_3, chemomechanical final polishing.
Ohmic Contact Material	Ga/In in eutectic form.
Potting Material	Epotek H20 E silver epoxy to a brass button. Brass button potted in Epotek 377 (an electrically and chemically resistive, high temperature epoxy).
Photoresist Mask Parameters	
Photoresist Material	Shipley 1400-31.
Prebake	Dehydration bake 110°C for 45 min. Cool to 18°-25°C ambient.
Coating	Static dispense, coat entire surface.
Ramp	Maximum possible (0.3 sec at EIC Labs).
Spin	5000 rpm for 25 sec.
Air Dry	10 min (to minimize radial pattern).
Softbake	30 min at 95 ± 1°C in convection oven. Cool to ambient.
Mask	2:1 line:space ratio, 50 cycles/mm, oriented in $[01\bar{1}]$ direction.
Exposure	Oriel 87000 series Deep UV Illuminator, 350-450 nm, ≈100 mW/cm^2 at sample, 5.7 sec typical exposure time.
Develop	Microposit CD-30 developer, full strength, immersion, 20-30 sec typical.
Hard Bake	120°C, 45 min, convection oven. Cool to ambient.
Photoelectrochemical Etching Parameters	
Electrolyte	0.05 M KCl solution adjusted to pH 3-4 with dilute HCl.
Reference Electrode	Saturated Calomel Electrode (SCE).
Counter Electrode	Nickel Mesh.
GaAs Potential	+0.4 V vs SCE.
Light Intensity	5-7 mW/cm^2, Oriel Illuminator.
Typical Photo Current	1.33 mA/cm^2 (no resist pattern on GaAs), ≈2.5-3.0 mA/cm^2 of exposed GaAs surface (with 2:1 resist mask pattern); would vary depending on the mask conditions.
Typical Dark Current	≈ 1 $\mu A/cm^2$.
Coulombs Required	(100) 10.65 C/cm^2 (100), 8.6 C/cm^2(100-18).
Typical Etch Time	≈ 3 hrs/cm^2.
Residual Photoresist Removal	Microposit 140 Remover or Acetone in an ultrasonic cleaner.

5.0 SUMMARY AND CONCLUSION

During this program we have developed a new, controllable process for fabricating blazed, V-groove diffraction gratings. The process is based on photoelectrochemical etching of a semiconductor with a Zn-blend lattice under conditions where the [111] surfaces become revealed due to their relatively slow photoetching rates. The process has been demonstrated for GaAs but, in principle, is possible for other semiconductors with similar crystal structures such as Si, GaP and InP.

The basic process for forming symmetrical groove profiles entails patterning a crystal with a periodic photoresist on the (100) surface in the [01$\bar{1}$] crystallographic direction. Photoelectrochemical etching of the exposed regions results in exposure of the [111]Ga or other Ga-rich planes, and eventual undercutting of the photoresist lines, resulting in formation of the continuous periodic grating structure. The process can be monitored coulometrically, and the experimental conditions "fine tuned" to produce the smoothest micromorphology.

Blazed gratings are of the greatest immediate interest to NASA. Table 7 lists the six fixed Echelles proposed by Woodgate for the STIS. These are all blazed, low pitch elements. We have developed a photoelectrochemical process for producing blazed gratings using crystals sliced at an appropriate angle off the (100) planar axis. We fabricated gratings on this program with blaze angles ranging from 30 to 44° or 43 to 60°, depending on the direction of light incidence with respect to the grating surface. We foresee no problem in fabricating structures with other blaze angles, including those listed in Table 7.

Table 7. Proposed Echelle Gratings for the Space Telescope Imaging Spectrograph

Grating	Order	λÅ	Blaze,°	Spacing (μm)	(100)/(011) angle, °
E1	159-258	1050-1700	70,20	14.5	25
E2	119-211	1700-3000	63,27	20.1	18
E3	31-50	1050-1700	26,64	6.1	19
E4	31-54	1700-3000	26,64	10.7	19
E5	31-62	3000-6000	26,64	21.3	19
E6	31-62	5500-11000	26,64	39.1	19

The general optical quality of the gratings has seen evolutionary improvement over the program duration, but is still not sufficient for inclusion in NASA instrumentation. One achievement has been to optimize the micromorphology of the groove walls. Several process variables must be considered when attempting to produce smooth-walled V-grooves in GaAs by photoelectrochemical etching. Of primary importance is the use of an electrolyte in which the oxidation products are soluble, such as aqueous KCl. However, the micromorphology is dependent on more subtle factors,

such as the relative stability of the oxide covered crystalline habits in the electrolyte. The use of an adsorbing electrolyte, such as Cl^-, also promotes a smooth morphology since it prevents a dissolution mechanism which depends on the localized breakdown of a passive film. Aqueous KCl, 0.05-0.1M, gives rise to the smoothest walls and angles closest to that of (111)Ga. Bias voltage and light intensity (current density) also affect morphology, with good results obtained at <0.5V (SCE) and average currents of about 1 mA/cm^2. These conditions of smooth morphology and predictable V-groove angle are particularly relevant to the production of diffraction gratings.

Most of the difficulties remaining at this point involve the macromorphology of the gratings, including flatness, long range uniformity, scratches and etch pits. A key consideration in developing this process is the uniformity of the photoresist application process. Considerable experimentation with dip coating has led us to the conclusion that a high degree of lateral uniformity is difficult to achieve by this technique, at least with the procedures employed here. Superior results were always obtained with spin coating, which may be suitable for gratings up to 6" x 6". It is still unclear, however, whether small variations in the uniformity of the photoresist thickness will affect the final product. Of paramount importance is that the spaces of the initial photoresist pattern be sharply defined, that the pattern be complete and uniform, and that the photoresist adhesion to the substrate be uniform.

Studies of GaAs surface preparation revealed that improvements in surface flatness are possible. However, at present the quality of GaAs is insufficient to guarantee that pits and dislocations will not be revealed by the etching process. The best GaAs available still has etch pit densities of $>10^3/cm^2$. This is to be compared to Si, which is available with zero etch pit density. In our studies, even under conditions where the micromorphology of the grating wall is excellent, the macromorphology caused by statistical numbers of etch pits was generally unacceptable. The regions giving rise to etch pits appear to have a different photoelectrochemical activity from the main bulk of the crystal. Although it is conceivable that process conditions could be designed to ameliorate this difference, these conditions have not yet been discovered.

In conclusion, the general outlook for photoelectrochemical etching as a means for the fabrication of high quality diffraction gratings is promising. Photoresist masks prepared by holographic techniques are expected to have the linear uniformity necessary to reduce spacing errors to acceptable values. A major factor in the commercial success of the technique is to acquire starting material of sufficiently high quality. As GaAs electronics technology evolves, material quality is liable to improve as well. Alternatively, other crystalline materials such as Si might be considered, which are available in higher quality. In the past, Si has been regarded as being more prone to surface passivation during photoanodic dissolution than GaAs. However, newly discovered electrolytes for Si photoetching are changing this picture.

6.0 REFERENCES

1. L. Comerford and P. Zory, Appl. Phys. Lett. 25, 208 (1974).
2. W. Tsang and S. Wang, Appl. Phys. Lett. 28, 44 (1976).
3. M.M. Carrabba, N.M. Nguyen and R.D. Rauh, Appl. Optics 25, 4516 (1986).
4. M.M. Carrabba, N.M. Nguyen and R.D. Rauh, Mat. Res. Soc. Symp. Proc. 75, 665 (1987).
5. J. Li, M.M. Carrabba, J.P. Hachey, S. Mathew and R.D. Rauh, J. Electrochem. Soc. 135, 3171 (1988).
6. M.M. Carrabba, N.M. Nguyen and R.D. Rauh, J. Electrochem. Soc. 134, 1855 (1987).
7. R. Matz, IEEE J. Lightwave Technol. LT-4, 726 (1986).
8. R. Matz and J. Zirrgiebel, J. Appl. Phys. 64, 3402 (1988).
9. Gallium Arsenide Processing Techniques, R.E. Williams, ed. (Dedham, MA: Artech House, Inc., 1984), Ch. II.5
10. M. Pourbaix, Atlas of Electrochemical Equilibria in Aqueous Solution (Oxford: Pergamon Press, 1966).
11. A.M. Dymov and A.P. Savostin, Analytical Chemistry of Gallium (Ann Arbor: Ann Arbor Science Publishers, 1970), p. 16.
12. K. Schwabe, Z. Phys. Chem. 217, 170 (1959).
13. P.A. Koh., C. Wolowodiuk and F.W. Ostermayer, Jr., J. Electrochem. Soc. 130, 2288 (1983).
14. See for example, H. Gerishcer, Ber. Bunsenges. Phys. Chem. 69, 578 (1965); J. Electrochem. Soc. 113, 1174 (1966); Surf. Sci. 13, 265 (1969).
15. D.W. Shaw, J. Electrochem. Soc. 128, 874 (1981).
16. D. Elliott, Microlithography: Process Technology for IC Fabrication (New York, NY: McGraw-Hill Book Company, 1986), p. 74.
17. S. Wolf and R.N. Tauber, Silicon Processing for the VLSI Era: Vol. 1 - Process Technology (Sunset Beach, CA: Lattice Press, 1986), p. 431.
18. "Dealing with the Unique Properties of GaAs," Surfacetech Review (Rodel Products Corporation), Vol. 1, Issue 4, p. 1.
19. "Analyzing the Components of Chemo-Mechanical Polishing," Surfacetech Review (Rodel Products Corporation), Vol. 1, Issue 5, p. 2.

7.0 APPENDIX A

Photoelectrochemical Fabrication of Sawtooth Gratings in n-GaAs, Applied Optics 25, 4516-4518, 1986.

Reprinted from Applied Optics, Vol. 25, Page 4516, December 15, 1986

Photoelectrochemical fabrication of sawtooth gratings in *n*-GaAs

Michael M. Carrabba, Nguyet M. Nguyen, and R. David Rauh

EIC Laboratories, Inc., 111 Downey Street, Norwood, Massachusetts 02062.

Received 23 August 1986.
0003-6935/86/244516-03$02.00/0.

Deep diffraction gratings with a low pitch (grooves/mm) are frequently employed in high performance spectroscopic instruments operating at high orders. Chemical etching offers one means of grating fabrication which has been used to form smooth groove surfaces with low light scattering.[1] Anisotropic etching in certain crystals can produce grooves with angled facets, and this method has been employed to make small area eschelles in silicon and GaAs.[2-6] These techniques utilize an oriented Ronchi ruling pattern of dielectric or photoresist to define the groove direction along the crystal surface. This mask is undercut as the etching proceeds to form sawteeth. To produce a uniform grating over a large area, it is necessary to have a uniform rate of etching over the entire surface, since there is no natural etch stop mechanism. Such uniformity may be difficult to achieve in chemical processes where the reaction and diffusion rates are sensitive to temperature and agitation of the etching solution. Furthermore, there is no present means of *in situ* monitoring of groove development in chemical etching processes.

We present here a means of fabricating V-groove grating structures using a photoelectrochemical approach. In this method, the grating is etched into the surface of a semiconductor with *n*-type doping. The semiconductor is mounted in an electrochemical cell containing an electrolyte and its potential controlled vs a reference electrode using a potentiostat. At positive potentials, a space charge region develops at the semiconductor–electrolyte interface with associated upward bending of the conduction and valence bands. When the semiconductor is irradiated with light of energy greater than its bandgap, holes (minority carriers) are produced in the valence band which diffuse to the surface under the internal field. For most semiconductors in most aqueous electrolytes, these holes are sufficiently energetic to decompose the crystal lattice, giving rise to oxidation products.[7] Modulated by the photon flux, etching will occur at the illuminated surface if the products are soluble in the electrolyte. Using this method, a number of workers have produced sinusoidal holographic gratings on a variety of semiconductors.[8,9]

Unlike Si, the oxidation products of III–V compounds like GaAs are soluble in water at pH 7, making photoelectrochemical etching possible without resorting to corrosive reactants. Thus, to investigate the photoelectrochemical technique for making low pitch gratings, polished single crystals of (100) oriented *n*-GaAs ($N_d = 1.4 \times 10^{17}$–2.0×10^{18} cm^{-3}, MA/COM Laser Diode, Inc.) were patterned along the [01$\bar{1}$] and [011] directions using a 100-cycle/mm Ronchi ruling mask. Shipley 1350J positive photoresist was employed and developed using the manufacturer's instructions. An ohmic contact was made on the unpolished face using a Ga/In eutectic, and the crystal was mounted in the electrochemical cell shown in Fig. 1. The electrolyte was either 1-M KCl or 0.5-M Tiron (4,5-dihydroxy-1,3-benzene disulfonic acid, disodium salt), a Ga^{3+} complexant,[10] yielding equivalent results. However, the Tiron is useful in enhancing the dissolution of passivating oxides that may form on the crystal sur-

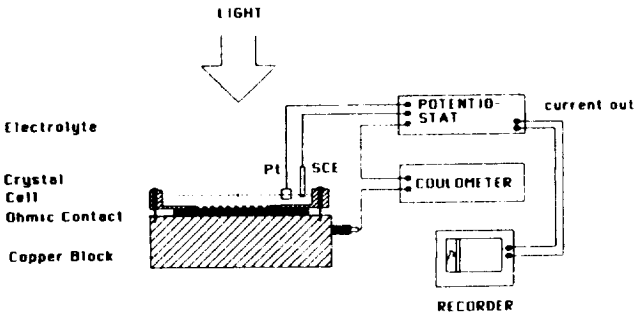

Fig. 1. Apparatus for photoelectrochemical etching.

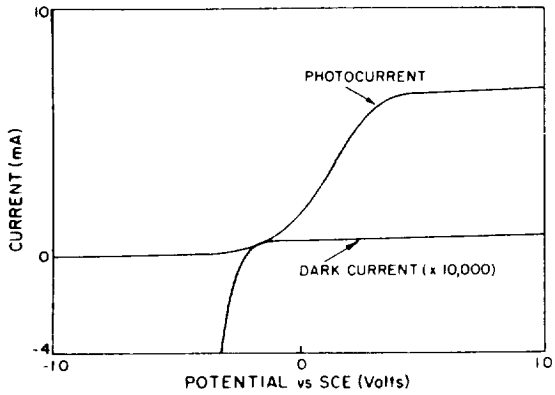

Fig. 2. Current-voltage curves for (100) n-GaAs in 0.5-M Tiron electrolyte. Curves are shown recorded in the dark and under illumination of a 100-W Xe source (200–300 mW/cm^2). Exposed crystal area = 0.2 cm^2.

face during postbaking of the resist pattern. The variation of current with applied voltage in the dark and under illumination is shown in Fig. 2. It is evident that the photocurrent reaches a photon-limited plateau of >0.5 V and that the dark current is very low out to >1 V. Photoelectrochemical etching of the patterned crystal surface was conducted in this plateau region at 0.7 V under the uniform illumination of a Xe-arc lamp. The time evolution of the photocurrent was used to monitor the etching process.

The result of etching the groove in the [01$\bar{1}$] direction was a sawtooth profile depicted in various stages of development in Fig. 3. Thus the etch profile is not determined solely by the photon flux in this case. The photocurrent increases gradually during the etching process, as shown in Fig. 4, due to the undercutting of the resist stripes by the growing sawtooth. A maximum is finally reached when the grating is complete. The groove angles are similar to those revealed by aggressive chemical etchants. Since the direction of photogeneration of holes is dictated by the light flux, the exposure of the (111) Ga plane must be due to a lower rate of trapping photogenerated minority carriers (holes) at this surface. Note that the depth of the etched features can be controlled by monitoring the total coulombs passed, while the rate of etching is precisely controlled by the light intensity. Symmetrical grooves spaced 10 μm apart will have a depth of 7.14 μm. The theoretical volume of GaAs removed to form these grooves over 1 cm^2 is 3.57 × 10^{-4} cm^3 or 8.07 C/cm^2 assuming 6 equivalents/mole.[11] Typically, we observed that 10–20% less total charge is required. This may be due to a lower stoichiometry for the dissolution reaction in the Tiron electrolyte.

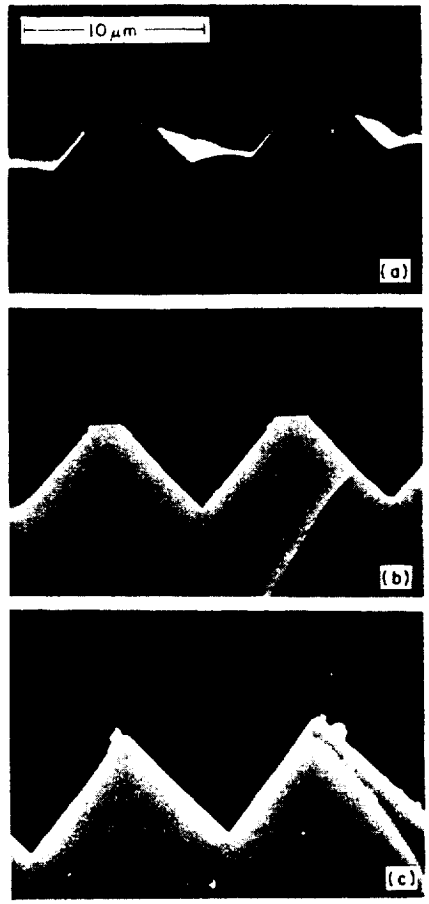

Fig. 3. Scanning electron micrographs showing cross sections of grooves photoelectrochemically etched in the (100) n-GaAs, [01$\bar{1}$] direction, at three stages of development.

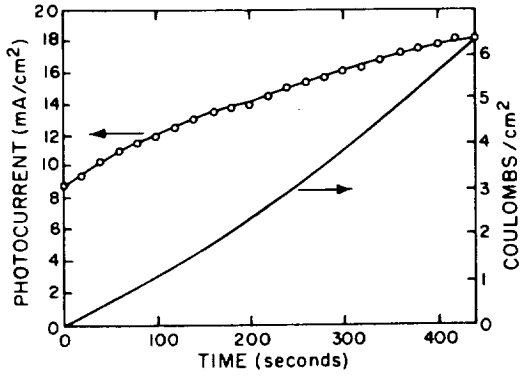

Fig. 4. Time evolution of photocurrent and charge for etching V-grooves in n-GaAs, shown in Fig. 3.

The gratings are characterized by exceptional smoothness, although etch pits may develop in defective crystals in some conditions.[10] The fact that the etching rate can be controlled means that diffusional gradients in the liquid, which may impair the uniformity, can be minimized. Similarly, an even distribution of light intensity over the crystal surface should impose a lateral homogeneity to the etching rate. Other angles and blazed groove profiles may be possible

using different crystal orientations, if results of chemical etching of different low index planes[4] are also observed for photoelectrochemical etching. It is important to note that the very mild electrolytes used in photoelectrochemical etching of GaAs are compatible with virtually all resist or mask materials.

Commercial availability of 10-cm (4-in.) GaAs wafers suggests that this material could be used for practical spectroscopic gratings. In addition, gratings with a variety of groove structures are used in integrated electrooptics which are mostly based on compound semiconductors.[12] An understanding of crystallographic effects in controlling groove geometry during photoetching will permit the fabrication of new structures with a high degree of process control.

This work was supported in part by the Office of Naval Research and the National Aeronautics and Space Administration.

References

1. M. Hutley, *Diffraction Gratings* (Academic, New York, 1982).
2. P. Philippe, S. Valette, O. Mata Mendez, and D. Maystre, "Wavelength Demultiplexer: Using Eschelette Gratings on Silicon Substrate," Appl. Opt. **24,** 1006 (1985).
3. S. Sriram and E. P. Supertzi, "Novel V Grooves in Silicon," Appl. Opt. **24,** 1784 (1985).
4. R. E. Williams, *Gallium Arsenide Processing Techniques* (Artech House, Dedham, MA, 1984), Chap. 5.
5. L. Comerford and P. Zory, "Selectively Etched Diffraction Gratings in GaAs," Appl. Phys. Lett. **25,** 208 (1974).
6. W. Tsang and S. Wang, "Profile and Groove-Depth Control in GaAs Diffraction Gratings Fabricated by Preferential Chemical Etching in H_2SO_4-H_2O_2-H_2O System," Appl. Phys. Lett. **28,** 44 (1976).
7. H. Gerischer, "On the Stability of Semiconductor Electrodes Against Photodecomposition," J. Electroanal. Chem. **82,** 133 (1977).
8. Y. Y. Gurevich and Y. V. Pleskov, "Photoelectrochemistry of Semiconductors," in *Semiconductors and Semimetals, Vol. 19,* R. K. Willardson and A. C. Beers, Eds. (Academic, New York, 1983).
9. R. Lum, A. Glass, F. Ostermayer, Jr., P. Kohl, A. Ballman, and R. Logan, "Holographic Photoelectrochemical Etching of Diffraction Gratings in *n*-InP and *n*-GaInAsP for Distributed Feedback Lasers," J. Appl. Phys. **57,** 39 (1985)
10. M. M. Faktor and J. L. Stevenson, "The Detection of Structural Defects in GaAs by Electrochemical Etching," J. Electrochem. Soc. **125,** 621 (1978).
11. H. Gerischer, "On the Mechanism of Anodic Dissolution of Gallium Arsenide," Ber. Bunsenges. **69,** 578 (1965).
12. T. Suhara and H. Nishihara, "Integrated Optics Components and Devices Using Periodic Structures," IEEE J. Quantum Electron. **QE-22,** 845 (1986).

8.0 APPENDIX B

Photoelectrochemical Etching of Blazed Echelle Gratings in n-GaAs, J. Electrochem. Soc. 35, 3170-3171, 1988.

Photoelectrochemical Etching of Blazed Echelle Gratings in n-GaAs

J. Li*, M. M. Carrabba, J. P. Hachey, S. Mathew, and R. D. Rauh*

EIC Laboratories, Incorporated, Norwood, Massachusetts 02062

INTRODUCTION

Photoelectrochemical etching can be a technique for producing microstructures in semiconductors with high aspect ratios and lateral uniformities. As an example of this application, we have reported recently on producing sawtooth Echelle diffraction gratings in (100) oriented crystals on n-GaAs using this method (1). These gratings are employed in a variety of electro-optical devices and in very high resolution spectrometers. Because of the large amount of material which must be removed in fabrication, they are difficult to produce with smooth walls by conventional ruling energies, particularly in the low groove densities frequently needed.

The etching process relies on the orientational dependence of photoelectrochemical dissolution of GaAs, which favors the (111)As over the (111)Ga polar face, similar to some types of oxidative chemical etching (2,3). Etching in the (100) surface necessarily results in symmetrical groove profiles, while most optical applications of gratings require unsymmetrical blazed structures. It is the purpose of this communication to report the photoelectrochemical fabrication of blazed, deep gratings with crystallographic control of the blaze angle.

EXPERIMENTAL

GaAs wafers (n-type, 5 x 10^{17} cm^{-3}) were cut from a boule supplied by Bertram Laboratories. Diced wafers of 5/8 x 5/8" dimensions were mounted as electrodes and then sequentially polished with alumina abrasives down to 0.05 μm, and finally chemomechanically polished with a silica/bleach slurry. Grating patterns were produced in positive photoresist (Shipley 1350J) with a periodicity of 50 cycles/mm. A line to space ratio of 2 was determined to give optimum results (4). Both the photoresist exposure and the photoelectrochemical etching were accomplished using a highly collimated UV source.

*Electrochemical Society Active Member

Key words: diffraction grating, gallium arsenide, etching, photoelectrochemical, crystallographic

(Oriel Corporation 87301 illuminator). All experiments were conducted with potentiostatic control in a 3-electrode cell with a standard calomel (SCE) reference electrode.

RESULTS AND DISCUSSION

In order to produce blazed Echelle gratings, it is necessary to cut the GaAs crystal at an angle off the (100) plane toward the (011) plane. Orienting the photoresist lines in the [01$\bar{1}$] direction should then give rise to structures with the interior angles governed by the preferred Ga-rich surfaces. One advantage of photoelectrochemical etching for producing these structures is that the process can be followed coulometrically. The charge, Q, required to etch the V-groove sawtooth pattern is:

$$Q(C/cm^2) = 3.54 \times 10^3 nN\left(\frac{0.5\ W^2}{\cot(\alpha-\beta)+\cot(\alpha+\beta)}\right) \quad [1]$$

Here, n is the electron stoichiometry (equivalents/mole) of the photoanodic dissolution reaction, W is the width (cm) of each groove, α is the angle of the groove face with respect to the (100) surface, β is the angle of the crystal slice with respect to the (100) surface, and N is the number of grooves/cm. In the present case, n = 6, N = 500 and W = 2 x 10^{-3} cm.

To demonstrate the photoelectrochemical etching of blazed structures, crystals were cut with (100), (100)-8° and (100)-18° orientations. The electrolyte composition was 0.1M KCl, adjusted to pH 3, and the light intensity was 30 mW/cm^2. The potential was held at the onset of the photon-limited region, 0.4V vs. SCE. Initial structures were etched under the assumption that the interior angles were 70.54°, as defined by the (111)Ga surfaces. However, we found under closer examination that this angle was dependent on the etching conditions and on the electrolyte, and was closer to 90° under the present conditions. This would correspond most closely to the (223)Ga-rich surface. With a 90° interior angle, equation [1] predicts a charge of 10.6 and 8.6 C/cm^2 required to etch the gratings in the (100) and

(100)-18° surfaces, respectively. With coulometric monitoring, both unblazed and blazed gratings were produced with pointed tops and bottoms and extremely smooth walls. A scanning electron micrograph (SEM) of the blazed structure from the (100)-18° surface is shown in Figure 1. The blaze angle of 60° is slightly less than the expected value of 63°, an error probably due to inaccuracies accumulated in the cutting and polishing procedures.

Since making cross sections for SEM analysis is a destructive technique, an optical method was developed for routine determination of the blaze angle. The gratings were mounted on a graduated turntable with the grooves parallel to the rotation axis, and illuminated with a He-Cd laser source (442 nm). The zero-order reflection was used as a reference point, i.e., when the grating is 90° with respect to the laser source. The grating was then rotated and the angles recorded which produced a back-reflected beam that passed the laser aperture. The angle of the brightest back-reflection is the blaze angle (θ_1). It can also be calculated from the order number (m) giving this strongest back-reflection, according to the grating equation

$$m\lambda = 2d\sin\theta \qquad [2]$$

where d is the groove spacing and λ the wavelength. Table 1 summarizes the blaze angles for several gratings measured from the turntable angle, from equation [2], and from SEM cross-section profiles. Also included in Table 1 are the complementary blaze angles, θ_2, measured by rotating the turntable in the opposite direction ($\theta_1 + \theta_2 \sim 90°$). It is seen that the three methods give results that are in excellent agreement.

Table 1. Properties of Photoelectrochemically Etched Echelle Gratings

Sample	Orders for θ_1/θ_2	Blaze Angle Turntable	Blaze Angle Eq.2	θ_1/θ_2 SEM	Theory
1	63/64	43/45	44/45	43/44	45/45
2	64/65	44/46	45/46	44/45	45/45
3	71/56	53/37	52/38	51/39	53/37
4	70/57	52/39	51/39	51/39	53/37
5	78/48	59/31	60/32	60/30	63/27

Sample key:
1. (100), 0.5 M KCl
2. (100), 0.1 M KCl
3. (100)-8°, 0.1 M KCl
4. (100)-8°, 1.0 M KCl
5. (100)-18°, 0.05 M KCl

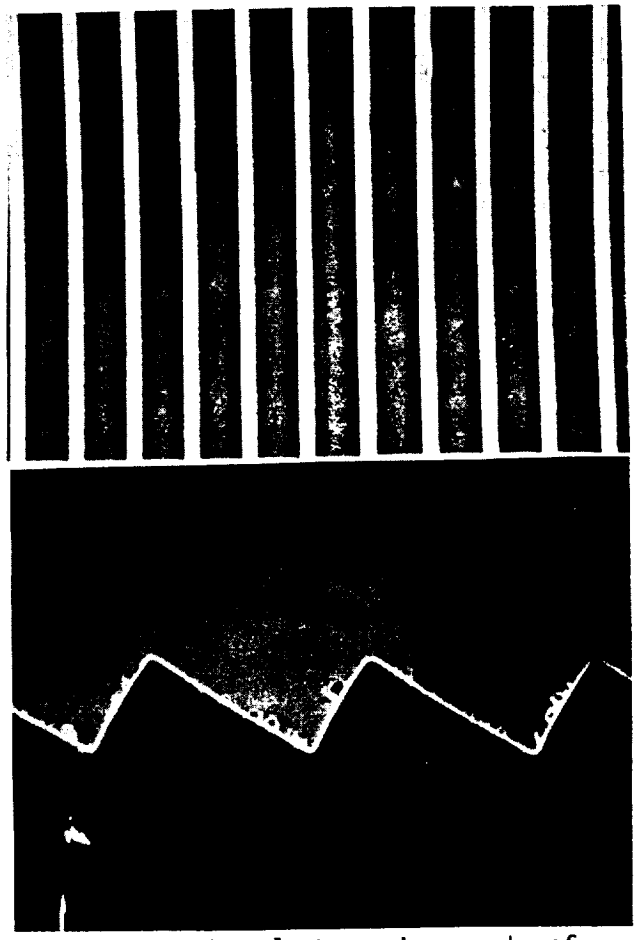

Fig. 1. Scanning electron micrographs of blazed Echelle gratings etched photoelectrochemically in the (100)-18° surface of n-GaAs. Groove spacing is 20 μm.

ACKNOWLEDGMENT

This work was supported by NASA and by the Office of Naval Research.

REFERENCES

1. M.M. Carrabba, N.M. Nguyen and R.D. Rauh, Appl. Optics, 25, 4516 (1986).
2. M.M. Carrabba, N.M. Nguyen and R.D. Rauh, This Journal, 134, 1855 (1987).
3. M.M. Carrabba, N.M. Nguyen and R.D. Rauh, Materials Research Society Symp. Proc., 75, 665 (1987).
4. J. Li, M.M. Carrabba and R.D. Rauh, unpublished results.

Manuscript received Aug. 9, 1988.
EIC Laboratories, Incorporated, assisted in meeting the publication costs of this article.

Reprinted from JOURNAL OF THE ELECTROCHEMICAL SOCIETY
Vol. 135, No. 12, December 1988
Printed in U.S.A.